photonics

Article

High Power Ytterbium-Doped Fiber Lasers Employing Longitudinal Vary Core Diameter Active Fibers

Lingfa Zeng [1], Xiaolin Wang [1,2,*], Yun Ye [1], Li Wang [1], Baolai Yang [1,2], Xiaoming Xi [1,2], Peng Wang [1,2], Zhiyong Pan [1,2], Hanwei Zhang [1,2], Chen Shi [1,2], Kai Han [1,2] and Xiaojun Xu [1,2]

[1] College of Advanced Interdisciplinary Studies, National University of Defense Technology, Changsha 410073, China
[2] Nanhu Laser Laboratory, Changsha 410073, China
* Correspondence: chinaphotonics@163.com

Abstract: Thanks to the advantage of balancing nonlinear effects and transverse mode instability, vary core diameter active fiber (VCAF) has been widely used in high power ytterbium-doped fiber lasers in recent years. Up to now, VCAF has developed from the basic form of the original tapered fiber to the spindle-shaped and saddle-shaped fiber with different characteristics and has been applied in conventional fiber lasers, oscillating–amplifying integrated fiber lasers, and quasi-continuous wave fiber lasers and successfully improved the performance of these lasers. In the present study, a 6110 W fiber laser amplifier is realized based on a tapered fiber. The maximum output power of a fiber laser amplifier based on spindle-shaped fibers is 6020 W with a beam quality of M^2~1.86. In this paper, we first introduce the basic concept of VCAF and summarize its main fabrication methods and advantages in high-power fiber laser applications. Then, we will present the recent research results of high-power fiber laser employing VCAF in our group and clarify the outstanding advantages of VCAF compared with the constant core diameter active fiber (CCAF).

Keywords: high-power fiber laser; vary core diameter active fiber; nonlinear effect; transverse mode instability

check for updates

Citation: Zeng, L.; Wang, X.; Ye, Y.; Wang, L.; Yang, B.; Xi, X.; Wang, P.; Pan, Z.; Zhang, H.; Shi, C.; et al. High Power Ytterbium-Doped Fiber Lasers Employing Longitudinal Vary Core Diameter Active Fibers. *Photonics* **2023**, *10*, 147. https://doi.org/10.3390/photonics10020147

Received: 25 December 2022
Revised: 21 January 2023
Accepted: 28 January 2023
Published: 31 January 2023

1. Introduction

High-power ytterbium-doped fiber lasers are widely used in industrial processing and other fields [1,2]. With the rapid development of double-cladding fiber, laser diode (LD) pumps, and fiber devices, the output power of fiber laser has been continuously improved, and fiber laser technology with an output power of several kilowatts or even 10 kilowatts has been relatively mature [3–7]. The special structure of fiber makes it easy to produce strong nonlinear effects under high-power conditions. Before 2010, the effective method to suppress nonlinear effects was to increase the core diameter of the fiber to reduce the laser power density in the core. At the same time, the control of the core diameter within a certain range will not have too much adverse impact on the laser beam quality. In 2010, the transverse mode instability (TMI) in large mode area fiber was first found and reported, which made it difficult to increase the output power by simply increasing the core diameter [8,9]. The development of high-power fiber lasers faces the problem of balancing nonlinear effects such as Stimulated Raman Scattering (SRS) and TMI [10,11]. In order to suppress the nonlinear effect or TMI, a lot of theoretical and experimental work has been carried out, including the optimization of pump wavelength, pump configuration, seed power, and the characteristics of active fiber [12–24].

The optimization of the structure of active fiber can be roughly divided into two aspects. One is to focus on the optimization of the transverse structure, such as the optimization of core diameter, core/cladding geometry, core-doping distribution, core refractive index distribution, etc. Typical examples are confined-doped fiber, chirally coupled-core (3C) fiber, and GTWave fiber [25–30]. The other direction is to focus on the optimization of the longitudinal structure, which is represented by the tapered fiber (TF). Conventional TF can be divided into short TF and long TF. The length of the short TF is basically in the order of centimeters, and this length is generally realized by stretching the constant core diameter fiber into a taper. The active TF that can be used in high-power fiber lasers is usually a long TF, and the length of the tapered section is usually several meters or more. The fiber laser based on TF can be traced back to 2008, when researchers from Tampere University of Technology in Finland first realized the TF-based laser oscillator with an 84 W laser output [31]. Benefiting from the good stimulated Brillouin scattering (SBS) suppression capability, TF is widely used in single frequency or narrow linewidth fiber lasers [32–38]. In 2020, the output power of single frequency fiber laser based on TF reached 550 W [37]. Among the reported single frequency or narrow linewidth fiber lasers, the fiber lengths in most studies are only several meters, except that the fiber lengths in Refs. [31,32] are more than 10 m; and the shortest is only 1.27 m. Most lasers can maintain near diffraction limit laser output.

Pulsed fiber laser is the most widely used field of TF by far, which is due to its good ability to suppress nonlinear effects and maintain beam quality [39–63]. In the existing reports, the center wavelength of the output laser of the Yb-doped TF-based pulsed fiber laser is usually 1030–1065 nm. The peak power of femtosecond pulse laser, picosecond pulse laser, and nanosecond pulse laser has reached 97 MW, 22 MW, and 375 kW, respectively [47,60,63]. The fiber length of TF used for pulsed fiber lasers is usually short, even less than 1 m. The core diameter of the small core diameter section of the fiber is usually about 10 µm, and the core diameter of the large core diameter section is generally more than 50 µm, or even 100 µm. However, the beam quality of the output laser can still maintain a near diffraction limit with a M^2 factor value of below 1.2. In addition, TF is also widely used in wide-linewidth, continuous-wave high-power fiber lasers. From 2008 to 2010, the researchers of the Tampere University of Technology reported on high-power fiber lasers based on TF, with the output power increasing from 84 W to 750 W [31,64–67]. In 2020, researchers of Huazhong University of Science and Technology realized 364 W laser output based on TF with a constant cladding diameter [68]. By 2022, they increased the output power of the same type of fiber to 2.7 kW, and the beam quality was about $M^2 = 2.16$ [69].

According to the structure of the fiber core along the longitudinal dimension, the commonly used tapered fiber can be regarded as a vary core diameter active fiber (VCAF) with a monotonically growing core diameter. In 2020, our group proposed VCAF represented by spindle-shaped fiber (SPF) and saddle-shaped fiber (SAF) and realized 3 kW and 1.3 kW all-fiber laser oscillators, respectively [70,71]. After that, VCAF, which is represented by SPF and TF, has received more and more attention in research. Based on VCAF with a constant core-to-cladding ratio, VCAF with constant cladding diameter has also been developed [72,73]. So far, there have been several publicly reported fiber lasers based on SPF with an output power of several kW, and the maximum output power has exceeded 6 kW [74–77]. Table 1 lists the main results of publicly reported VCAF-based fiber lasers. It can be seen that the high-average power fiber laser based on VCAF has developed rapidly in recent years.

From Table 1, we know that the VCAF were widely used in both continuous wave (CW) and pulsed fiber laser. In pulsed laser, peak power as high as 97 MW after compression was demonstrated in 2021. In the CW range, average power of up to 6020 W was demonstrated in 2022. In this paper, we will mainly introduce our latest work on VCAF. Firstly, the main advantages and fabrication methods of VCAF are briefly introduced. Then, our research in conventional fiber lasers based on VCAF is introduced. Finally, the applications of VCAF in new-type fiber lasers such as quasi-continuous wave (QCW) fiber laser, oscillating-amplifying integrated fiber laser (OAIFL), and bidirectional-output fiber laser are introduced. It is worth noting that all VCAF used in our experiment are double-cladding ytterbium-doped fibers.

Table 1. Summary of main results of fiber laser based on VCAF (SPF: spindle-shaped fiber; SAF: saddle-shaped fiber).

Year	Fiber Type	Core/Cladding Diameter	Fiber Length	Power (Average/Peak Power)	Affiliation *	Reference
2008	TF	5.6/174–27/834 µm	10.5 m	84 W @average	TUT	[31]
2008	TF	6.5/200–27/834 µm	12 m	212 W @average	TUT	[64]
2009	TF	10.8/145–65/835 µm	24 m	600 W @average	TUT	[65]
2010	TF	15/160–83/880 µm	6.3 m	24.3 kW	TUT	[40]
2010	TF	17.7/320–51.6/930 µm	23.5 m	750 W @average	TUT	[67]
2012	TF	7.5/120–44µm/700 µm	18 m	110 W @average	TUT	[78]
2013	TF	7.5/120–44/700 µm	18 m	160 W @average	RAS	[32]
2014	TF	9/145–50/800 µm	4 m	60 W/0.4 MW	TUT	[40]
2015	TF	10/80–45/430 µm	2.1 m	2.5 MW	RAS	[41]
2016	TF	10/237.1–46.9/579.9 µm	7 m	53 W @average	NUDT	[33]
2016	TF	25/250–60/600 µm	2 m	10.2 W/340 kW	The Aerospace Corporation	[42]
2016	TF	13–100 µm (core diameter)	6 m	5 MW	TUT	[79]
2017	TF	35/250–56/400 µm	2.8 m	1.5 MW	INO	[43]
2017	TF	6.9/29–45/190 µm	68 cm	11.4 W/167 kW	IPHT	[44]
2017	TF	6.5/53–56/460 µm	60 cm	10 W/230 kW	IPHT	[45]
2017	TF	10/72.5–62/450 µm	2 m	0.76 MW 22 MW after compression	RAS	[48]
2017	TF	18/145–100/800 µm	4 m	5 MW	Ampliconyx Ltd.	[48]
2017	TF	20–67 µm (core diameter)	2.2 m	1.5 MW	RAS	[49]
2017	TF	13.2/110–96/792 µm		70 W @average	Ampliconyx Ltd.	[50]
2017	TF	9–22 µm (core diameter)	2.5 m	120 W @average	ALPhANOV	[34]
2017	TF	35/250 to 56/400 µm	2.8 m	100 W @average	INO	[43]
2017	TF	21.2/417.3–30.4/609.6 µm	33 m	1470 W @average	NUDT	[80]
2018	TF	20/400–30/600 µm	33 m	260 W @average	NUDT	[81]
2018	TF	13.3/110–96/792 µm	3.6 m	28 W/292 kW	TUT	[51]
2018	TF	20/237.1–46.9/579.9 µm	7.2 m	260 W @average	NUDT	[36]
2018	TF	22.5/90–86/350 µm	2.5 m	19 W/107 kW	MIPT	[52]
2018	TF	12/53–45/200 µm	50 cm	15.5 W/375 kW	IPHT	[63]
2019	TF	36/250–58/560 µm	0.74 m	8.8 W/30 kW	NUDT	[54]
2019	TF	8.6/73–65/550 µm	2.7 m	44 W/550 kW	RAS	[55]
2019	TF	22/75–75/256 µm	3.2 m	10 MW after compression	RAS	[56]
2019	TF	7.2/57–43/344 µm	3 m	71 W/820 kW	RAS	[57]
2019	TF	35/280–100/800 µm	3.4 m	55 W @average	Ampliconyx Ltd.	[56]
2019	TF	17/170–49/490 µm	1.2 m	2.2 kW @PM, 4 kW @NPM	TU	[82]
2019	TF	36/250–58/560 µm	0.74 m	8.8 W/30 kW	NUDT	[83]
2019	TF	20/400–30/600 µm	33 m	1700 W @average	NUDT	[84]
2019	TF	20/400–30/600 µm	22 m	2170 W @average	NUDT	[85]
2020	TF	15/120–35/285 µm	2.8 m	72.5 W @average	TU	[86]
2020	TF	10/100–50/100 µm	2.5 m	7.5 W/1.26 MW	SPbPU	[59]
2020	TF	8.5/35.7–52/226.8 µm	4 cm	2.3 MW	IPHT	[58]
2020	SPF	20/400–30/600–20/400 µm	31 m	1836 W @average	NUDT	[87]

Table 1. *Cont.*

Year	Fiber Type	Core/Cladding Diameter	Fiber Length	Power (Average/Peak Power)	Affiliation *	Reference
2020	SPF	24.08/400–31/400–23.36/400 μm	25 m	2023 W @average	NUDT	[88]
2020	SPF	24.08/400–31/400–23.36/400 μm	25 m	3420 W @average	NUDT	[72]
2020	SPF	20/400–30/600–20/400 μm	30.5 m	3004 W @average	NUDT	[70]
2020	SAF	30.77/400–23.28/400–30.77/400 μm	22.8 m	1300 W @average	NUDT	[71]
2021	TF	31.2/400–52.5/400 μm	7 m	364 W @average	HUST	[68]
2021	TF	10/80–45/435 μm	2.6 m	97 MW after compression	Lumibird	[60]
2021	TF	10/70–59/432 μm	2.5 m	170 kW	CEA	[61]
2021	TF	10/100–50/500 μm	3 m	150 W/170 kW	SPbPU	[62]
2021	TF	15/120–35/285 μm	3 m	50 W/47 kW	TU	[89]
2021	TF	8/90–44/486 μm	6.7 m	64 W @average	TU	[90]
2021	TF	9.5/68–46/330 μm	2.45 m	150 W/0.74 MW	RAS	[91]
2021	SPF	22/413–32/600–22/413 μm	21 m	4000 W @average	NUDT	[74]
2021	SPF	27/410–39.5/410–27/410 μm	21 m	5008 W @average	NUDT	[92]
2022	TF	36.1/249.3–57.8/397.3 μm	1.27 m	141 W/1.3 MW	NUDT	[93]
2022	SPF	20/400–30/600–20/400 μm	19 m	4180 W @average	NUDT	[75]
2022	TF	35/250–56.2/400 μm	3.8 m	694 W @average	NUDT	[94]
2022	SPF	25/400–37.5/600–25/400 μm	27 m	4180 W @average	HUST	[76]
2022	TF	24/400–31/400 μm	16 m	2704 W @average	HUST	[69]
2022	TF	20/400–30/600 μm	17 m	4089 W @average	NUDT	[95]
2022	SPF	20.8/600–36/600–20.3/600 μm	28.5 m	2494 W @average	NUDT	[73]
2022	SPF	25/400–37.5/600–25/400 μm	24 m	6.4 kW QCW	NUDT	[96]
2022	SPF	25/400–37.5/600–25/400 μm	24 m	7.3 kW QCW	NUDT	[97]
2022	SPF	25/400–37.5/600–25/400 μm	21 m	6020 W @average	NUDT	[77]

* TUT: Tampere University of Technology; RAS: Russian Academy of Sciences; NUDT: National University of Defense Technology; IPHT: Leibniz Institute of Photonic Technology; TU: Tampere University; MIPT: Moscow Institute of Physics and Technology; SPbPU: Peter the Great Saint-Petersburg Polytechnic University; CEA: Commissariat à l'Energie Atomique et aux Energies Alternatives; HUST: Huazhong University Of Science And Technology.

2. Basic Concept of Vary Core Diameter Ytterbium-Doped Fiber

2.1. Classification of Vary Core Diameter Ytterbium-Doped Fiber

In high-power fiber lasers, a double-cladding Yb-doped fiber with a cross-section divided into three parts—core, inner cladding, and coating layer (outer cladding)—is generally used. The main feature of the VCAF that differs from conventional fibers is the gradual change in core diameter along the longitudinal direction. VCAF can be divided into three categories according to the form of fiber core diameter variation: tapered fiber (TF), spindle-shaped fiber (SPF), and saddle-shaped fiber (SAF), the structures of which are shown in Figure 1a–c, respectively. According to the fiber diameter distribution along the longitudinal direction, the VCAF can usually be divided into several sections. Among them, the TF includes the small core diameter section (S section), the gradient tapered section (T section), and the large core diameter section (L section), as shown in Figure 1a. The SPF includes two small core diameter sections, the S1 section and the S2 section, at both ends; a large core diameter section, the L section, in the middle; and the gradient-tapered sections, the T1 section and the T2 section, which connect the S1 section and the L section and connect the S2 section and the L section, as shown in Figure 1b. The SAF includes two large core diameter sections, the L1 section and the L2 section, at both ends; a small core diameter section, the S section, in the middle; and the gradient-tapered sections, the T1 section and the T2 section, which connect the L1 section and the S section and connect the L2 section and the S section, as shown in Figure 1c. In practical applications, T sections are often present in various fibers, whereas the L section or the S section can be removed as required. Based on core diameter variation, the inner cladding diameter of the VCAF can be kept constant or changing synchronously with the core at a constant core-to-cladding ratio. Both different types of VCAF can be widely used in high-power fiber lasers.

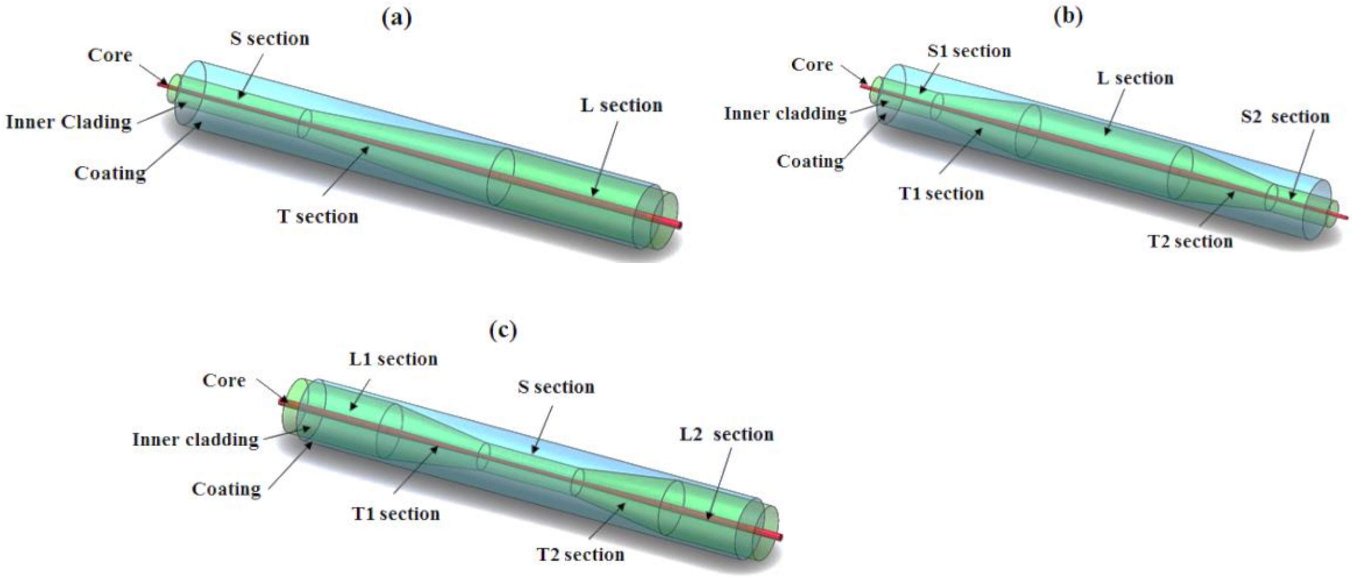

Figure 1. Scheme of the VCAF. (**a**) Tapered fiber (TF); (**b**) spindle-shaped fiber (SPF); (**c**) saddle-shaped fiber (SAF).

2.2. Advantages of VCAF

2.2.1. High Nonlinear Effect Threshold

VCAF can improve the nonlinear effect characteristics of the fiber laser benefit from the T-section as well as the L-section in the fiber. For single-frequency lasers, the changing core diameter reduces the changing of the Brillouin frequency shift and then broadens the SBS gain spectrum, which is helpful to increase the power of single-frequency lasers [98]. For wide-bandwidth continuous-wave fiber lasers, VCAF have a larger equivalent core diameter, which can reduce the laser power density in the core and suppress nonlinear effects such as SRS.

2.2.2. Good Mode Control Ability

In addition to good nonlinear effect characteristics, VCAF also has good mode control capability, which is reflected mainly in the following aspects. First, the presence of one or more S sections along the longitudinal direction, which supports fewer modes, combined with effective mode control methods such as fiber coiling can further suppress higher-order modes and effectively suppress TMI. Secondly, the T section of the fiber has a length of several meters, which is essentially a mode field adapter (MFA) with good beam-quality retention. Finally, the variation of core diameter along the longitudinal direction leads to a gradual variation of the difference between the propagation constants of fundamental and higher-order modes along the longitudinal direction of the fiber, which can reduce the interference between different transverse modes of the laser transmitted in the fiber and maintain a good beam quality.

2.2.3. Excellent ASE Inhibition

The presence of the T section in the VCAF allows ASE to leak from the core to the cladding during transmission, which can effectively suppress ASE. Taking the TF-based amplifier as an example, under normal conditions, the laser is transmitted and amplified from the S section to the L section, whereas the ASE is transmitted mainly backwards, that is, from the L section to the S section. The spontaneous emission in the T section near the L section initially occurs at an angle α ($\mathrm{NA}/T < \alpha < \mathrm{NA}$, where T is the fiber core cone ratio and NA is the numerical aperture of the fiber), and the ASE leaks from the core into the cladding after a short transmission distance from the L section. Therefore, VCAF can effectively suppress ASE, which is particularly beneficial for pulsed laser generation with low repetition frequency. With this type of fiber, researchers achieved a Q-switched pulsed laser output with a repetition frequency of 5 Hz. The peak power of the pulse is 24.3 kW with a pulse width and energy of 64 ns and 1.6 mJ [99].

2.3. Fabrication Process of VCAF

Traditional TF has a short T section, which is achieved by stretching the fiber with a constant core diameter by a taper machine, and the stroke of the equipment is usually below 1 m. Unlike short TF, it is difficult for VCAF to meet the requirements of general taper-pulling equipment due to the long length of the T section, and their fabrication is generally accomplished by fiber preform or fiber drawing. The specific fabrication methods include the preform form control method, the variable-speed drawing method, and the combination of the preform form control method and the variable-speed drawing method.

2.3.1. Preform Form Control Method

The preform form control method can be used for manufacturing VCAF with a constant cladding diameter [68]. The main steps of the method are shown in Figure 2. In the first step, conventional fiber preforms with a constant core diameter are fabricated using conventional preform fabrication methods (including modified chemical vapor deposition (MCVD), surface plasma chemical vapor deposition (SPCVD), etc.), as shown in Figure 2a. In the second step, the prepared preform is pre-tapered to obtain preform with multiple taper sections, as shown in Figure 2b. In the third step, the surface of the preform is ground and polished to obtain a constant distribution of the inner cladding diameter, as shown in Figure 2c. In the fourth step, the polished preform is cased to obtain a fiber preform with a suitable core-to-cladding ratio, as shown in Figure 2d, which completes the fabrication of the preform with different lengths and different T sections. Finally, the fiber preform is drawn at a constant speed using the drawing tower, and the fiber is coated during the drawing process to obtain the VCAF shown in Figure 2e.

2.3.2. Variable-Speed Drawing Method

Variable-speed drawing method is the simplest and most effective way to achieve VCAF with simultaneous variation of core and cladding diameters. With a defined core and cladding diameter of the preform, the cladding diameter (d) of the fiber is inversely related to the drawing speed as follows.

$$d(z,t) = \frac{K}{\nu_{\mathrm{T}}(z,t)} \tag{1}$$

where K is the scale factor associated with the drawing tower, z is the length of the drawn fiber, and t is the drawing time. The process of the variable-speed drawing method can be simply represented as in Figure 3. In the first step, preforms are manufactured using conventional processes based on designed fiber parameters such as doping and core/cladding diameter. In the second step, the preform is placed on the drawing tower, and the fiber core and cladding diameter are controlled by controlling the drawing speed. Taking the SPF shown in Figure 3 as an example, its five sections are used with different drawing speeds, where the speed of the S section is v_1, the speed of the L section is v_3, and the speed of the T section is $v_{(1–3)}(t)$ and $v_{(3–1)}(t)$, satisfying Equation (2):

$$\begin{cases} \frac{v_1}{v_3} = \frac{d_{L3}}{d_{S1}} \\ v_{(1-3)}(0) = v_1,\ v_{(1-3)}(T_1) = v_3 \\ v_{(3-1)}(0) = v_3,\ v_{(3-1)}(T_2) = v_1 \end{cases} \quad (2)$$

where d_{S1} and d_{L3} are the diameters of the S section and the L section, respectively. T_1, T_2 is the length of the 2 T sections. In the third step, the fiber is coated during the drawing process to obtain a VCAF with a constant core-to-cladding ratio. In general coating equipment, because the coating diameter cannot be changed online, the coating thickness at different positions of the fiber is different, so the outer diameter of the fiber is basically the same throughout the fiber length.

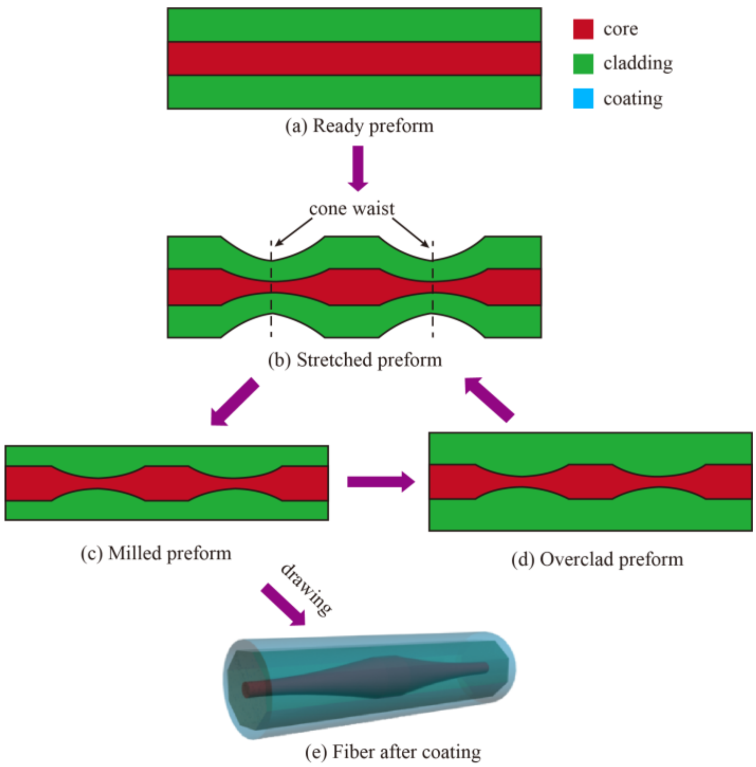

Figure 2. Schematic diagram of the VCAF in different preparation processes based on preform form control method.

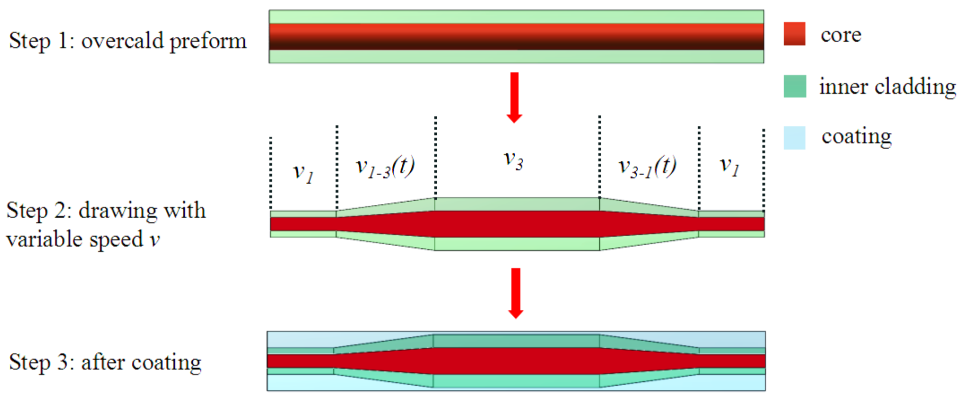

Figure 3. Schematic diagram of the VCAF in preparation processes based on variable-speed drawing method.

2.3.3. Combination of Preform Form Control and Variable-Speed Drawing Method

In fact, both the preform form control method and the variable-speed drawing method need to go through two processes: preform fabrication and fiber drawing. The fabrication of more different forms of VCAF can be achieved by combining the two methods. As shown in Figure 4, in the first step, common preforms are manufactured using conventional processes. The second step is to polish the preform after casing to obtain a preform with constant core diameter and variable cladding. The third step is to perform variable-speed drawing on the preform. During this process, the cladding diameter is ensured to be constant by speed control, and the final fiber core naturally changes gradually. The fourth step is to coat the fiber during the drawing process to obtain a VCAF with a constant cladding diameter. If a constant speed is used for drawing in the second step, it is also possible to obtain fibers with constant core diameter and variable cladding diameter.

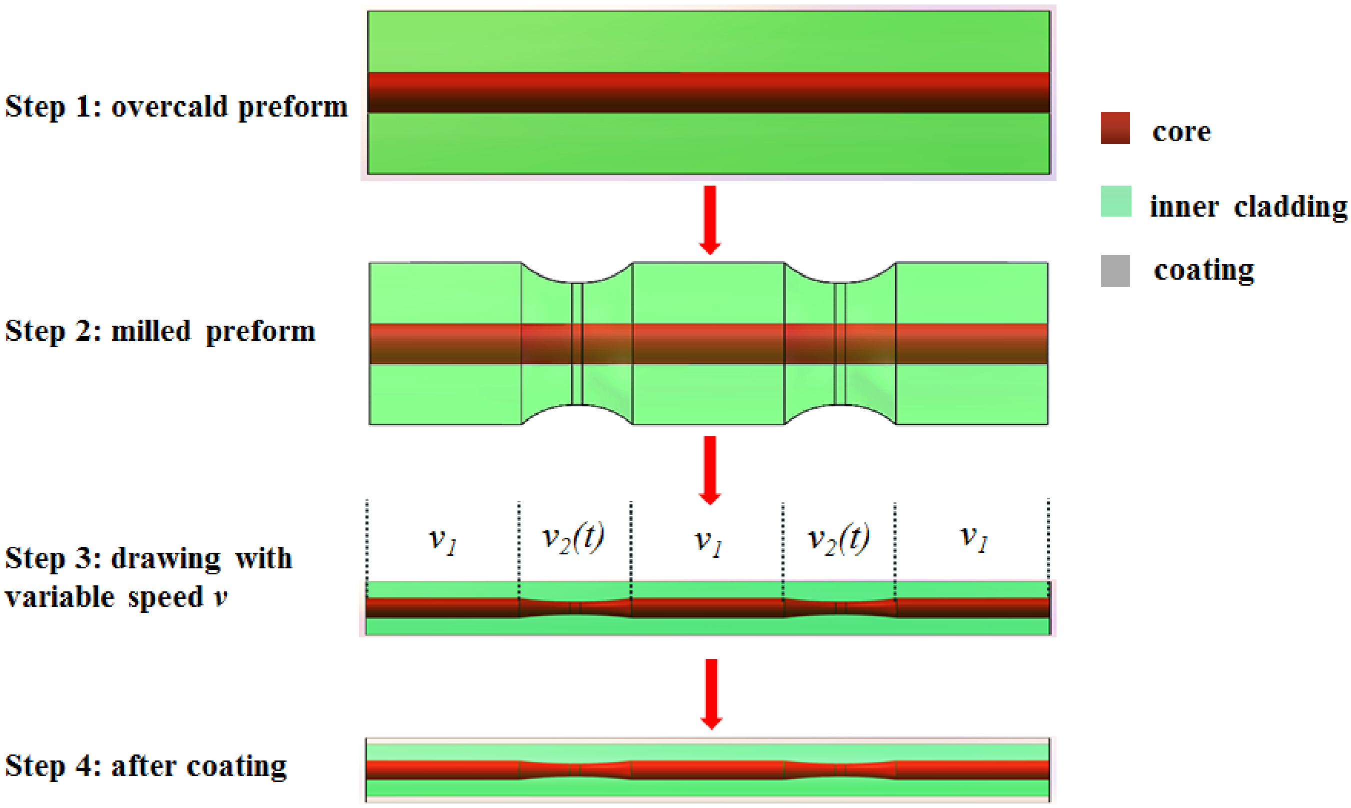

Figure 4. Schematic diagram of the variety core diameter fiber in preparation processes based on preform form control and drawing with variable speed method.

3. Simulation of SRS and TMI Characteristics of VCAF

In 2019, we conducted a theoretical study of SRS in TF-based fiber laser amplifiers for different morphologies (concave, linear, and convex) of TF, and the results showed that the convex TF has the best suppression of SRS thanks to the larger equivalent core diameter [100]. In fact, the S section in VCAF is helpful for the mitigation of TMI, whereas the L section can suppress the SRS. Therefore, the VCAF can balance SRS and TMI. Here, the balance function for TMI and SRS of VCAF will be briefly explained from the perspective of numerical simulation.

3.1. SRS in VCAF- and CCAF-Based Fiber Laser Oscillator

The rate equations of fiber lasers have become very mature theoretical tools. On this basis, our group has developed the fiber laser simulation software named SeeFiberLaser, which can be used to guide the theoretical research and experimental design of fiber lasers [101]. Taking the SPF as an example, we have conducted a theoretical study of SRS in fiber laser oscillators based on SPF and constant core diameter active fiber (CCAF) with different diameters, respectively, by using rate equations model of fiber lasers [100]. The structural parameters of the four fibers for simulation are shown in Table 2. Among them, fiber1–3 are CCAFs, fiber4 is an SPF, and the other simulated parameters are identical. In the simulation, three pumping configurations (forward pump (FP), backward pump (BP), and bidirectional pump (BIP)) are applied for different fibers. Table 3 lists the main parameters involved in the simulation and corresponding values. In the subsequent results, FP represents the application of forward pump configuration, BP represents the application of backward pump configuration, and BIP represents the application of bidirectional pump configuration.

Table 2. Parameters of several fibers used in simulation.

Fiber	Core Diameter/μm	Cladding Diameter/μm	Length/m
fiber1	20	400	11
fiber2	25	500	11
fiber3	30	600	11
fiber4	20–30–20	400–600–400	11

Table 3. Main parameters and values involved in theoretical simulation.

Parameter	Value	Parameter	Value
Signal center wavelength	1080 nm	Pump wavelength	976 nm
Length of passive fiber	10 m	Doping concentration	1.26×10^{26} m^{-3}
Signal range	1050 nm–1150 nm	Raman range	1116 nm–1150 nm
Raman power	$\sum_{\lambda = 1116\text{nm}}^{1150\text{nm}} P(\lambda)d\lambda$ ($P(\lambda)$ indicates signal power)		
Raman ratio	$(Raman\ power)/\sum_{\lambda = 1050\text{nm}}^{1150\text{nm}} P(\lambda)d\lambda$		
Pump configuration and pump power	FP, 5000 W BP, 5000 W BIP, 2500 W for FP and 2500 W for BP		

The equivalent core diameter of the SPF used is 24 μm, according to the calculation of the equivalent core diameter in ref. [72]. The simulation results of the fiber oscillator based on different fibers under different pump configurations are shown in Figure 5 and Table 4. Under the same conditions, the suppression ability of fiber4 (SPF) for the SRS is between fiber1 and fiber3 and is comparable to fiber2, the diameter of which is close to its equivalent core diameter. Consistent conclusions were also drawn on the spectra from the output lasers of the active and passive fibers.

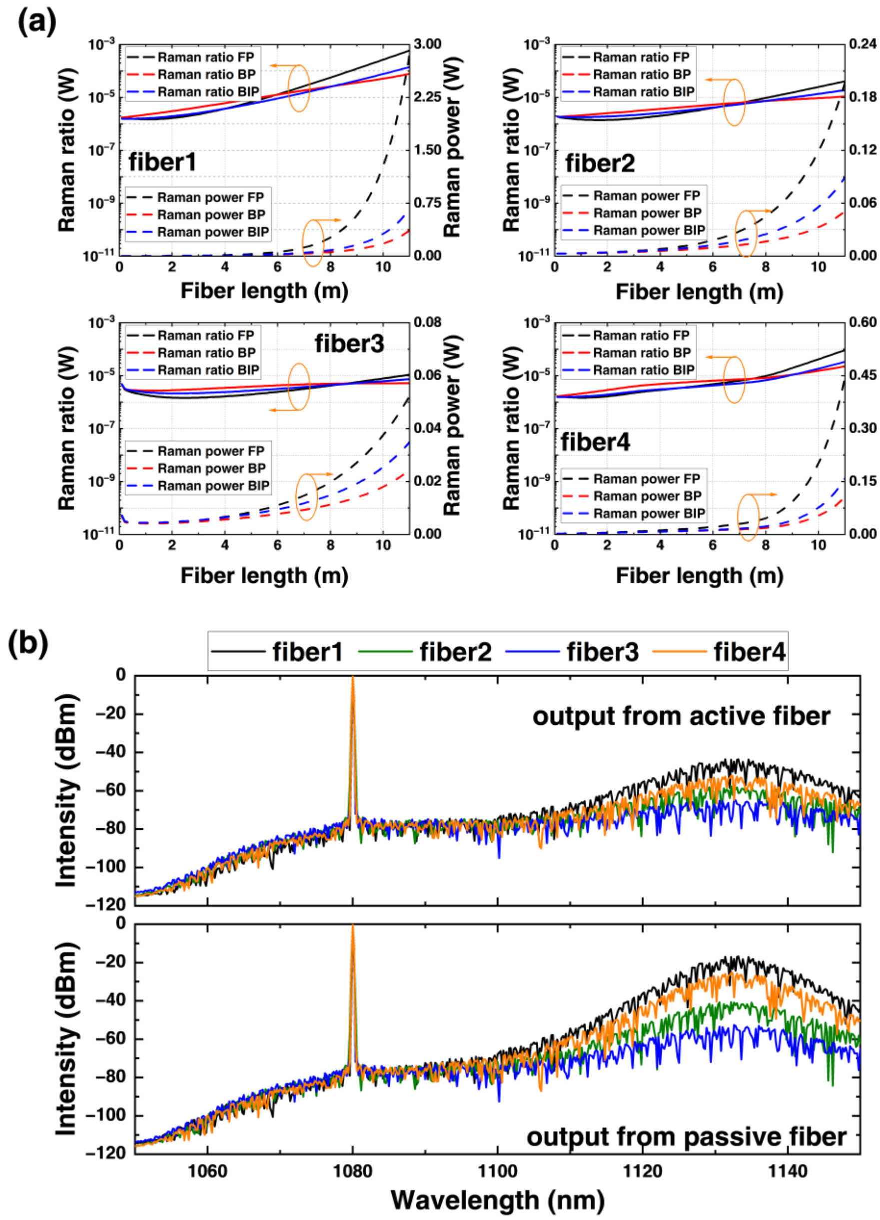

Figure 5. Simulation results of fiber laser oscillators based on different fibers. (**a**) The distribution of Raman power and Raman ratio along the fiber length in different fibers under different pump configurations. (**b**) The spectra of the output laser from the active and passive fibers.

Table 4. SRS simulation results in different fibers.

Fiber	Raman Power (W)			Raman Ratio ($\times 10^{-5}$)		
	FP	BP	BIP	FP	BP	BIP
fiber1	2.87	0.368	0.673	59.58	7.80	14.17
fiber2	0.20	0.051	0.089	4.09	1.08	1.89
fiber3	0.05	0.025	0.03	1.09	0.521	0.74
fiber4	0.45	0.107	0.16	9.23	2.28	3.35

3.2. Theoretical Comparison of TMI in Fiber Laser Amplifier Based on VCAF and CCAF

Here, the theory study of TMI effect employing three different fibers will be compared in a fiber amplifier. The first fiber is CCAF with a core/cladding diameter of 25/500 µm

(CCAF, 25/500). The second fiber is TF with a gradual core and cladding diameter change from 20/400 µm to 30/600 µm; the TF is a constant core-to-cladding ratio taper (TF-CCCR, TF1, 20/400–30/600). The third fiber is TF with a gradual core and cladding diameter change from 20/500 µm to 30/500 µm; the TF is tapered in core while constant in cladding, also called vary core-to-cladding ratio TF (TF-VCCR, TF2, 20/500–30/500).

Figure 6a,b shows the nonlinear coupling coefficients and the maximum coupling frequency shifts of the three fibers at 1000 W pump power in the fiber amplifier. It can be found that the nonlinear coupling coefficients within the three fibers decrease significantly and rapidly in the first 1 m of the fiber. It is also noted that the nonlinear coupling coefficient is smallest for the TF1, followed by the CCAF, and the largest for the TF2. The maximum coupling frequency shifts of the three fibers along the fiber length are shown in Figure 6b, which shows that for the two TF, the maximum coupling frequency shifts also change gradually with the fiber position as the fiber core diameter changes gradually along the fiber longitudinal position, and the maximum coupling frequency shifts decrease as the core diameter increases. The nonlinear coupling coefficient is multiplied with the fundamental mode power and integrated along the longitudinal direction of the fiber to obtain the equivalent coupling coefficient curves of the fiber under different frequency shifts, as shown in Figure 6c. The results in the figure show that the equivalent gain curve of the TF1 is significantly lower than that of both the TF2 and the CCAF, indicating that the TF2 is more favorable for suppressing mode coupling. In fact, in TF2, the TMI coupling coefficient is reduced because of the gradually increased absorption coefficient, which results in a smaller pump absorption in the first half of the fiber than in the second half, thus transferring the overall gain of the signal to the output end of the fiber and balancing the thermal load of the whole fiber. Figure 6d shows the evolution of the higher-order mode power ratio at the fiber output as the output power increases for the three fibers. It can be seen from the figure that under the forward pump configuration, the TF2 has the highest TMI threshold, followed by the TF1, and the CCAF fiber is the worst. Compared with the CCAF, the TMI thresholds of the TF2 and TF1 are improved by 40.6% and 5.97%, respectively, indicating that the TF has a great advantage in improving the TMI threshold under the same conditions.

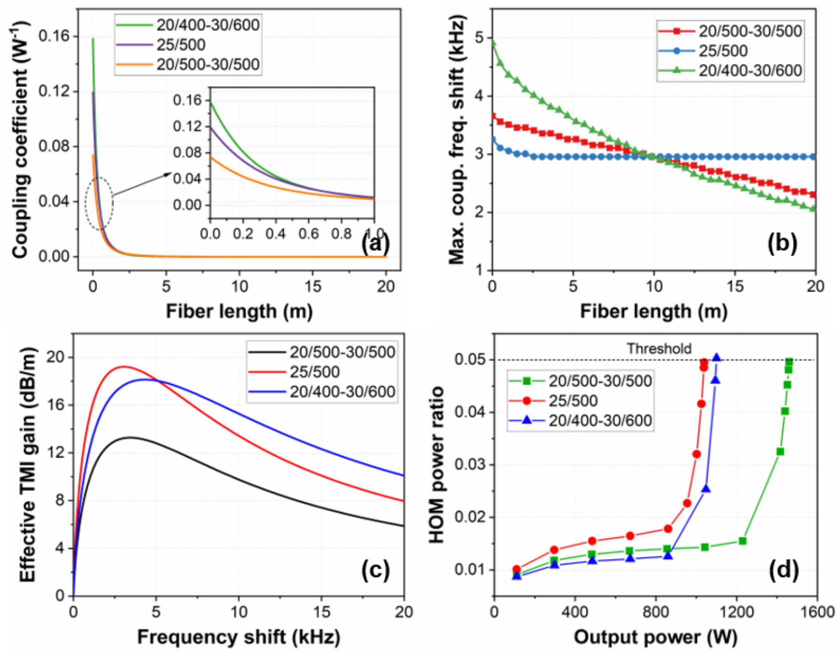

Figure 6. TMI simulation results for three fibers under forward pump configuration. (**a**) The nonlinear coupling coefficient, (**b**) the variation of maximum coupling frequency shift, (**c**) the equivalent TMI gain curve, and (**d**) the higher order mode (HOM) power ratio at the output end.

The above simulation results can illustrate the ability of VCAF to balance SRS and TMI in fiber lasers. The VCAF-based fiber laser has a similar ability to suppress SRS as a uniform fiber with the same equivalent core diameter. However, the TMI threshold of fiber laser based on VCAF is higher than that of uniform fiber with the same equivalent core diameter. The above simulation results only show typical comparison results. In fact, the structural parameters of VCAF, such as the core diameter and length of different sections, will affect the TMI and SRS of the laser. In practical applications, it can be optimized according to the actual needs to achieve higher power output.

4. Experimental Study on High-Power CW Fiber Laser Based on VCAF

4.1. Fiber Laser Based on TF with Constant Core-to-Cladding Ratio (TF-CCCR)

TF with a constant core-to-cladding ratio (TF-CCCR) is the most readily available of the VCAF and was the first to be used in experiments. Prior to 2019, most publicly reported TF-based fiber lasers focused on the field of pulsed lasers, and in the few studies of CW fiber lasers based on TF, the maximum laser output power was only 750 W, which was reported in 2010, when TMI in high-power fiber lasers had just been discovered [67].

4.1.1. High-Power Fiber Laser Oscillator Based on TF-CCCR

Starting from the balanced characteristics of TF for SRS and TMI, we conducted a TF-CCCR-based fiber laser oscillator in 2019 and achieved a 1.7 kW laser output [84]. The structure of the laser is shown in Figure 7. The total length of the TF used is about 33 m, and its core/cladding diameter gradually transitions from 20/400 μm to 30/600 μm, without the S section and the L section. A high-reflectivity fiber Bragg grating (HR FBG) with a core/cladding diameter of 20/400 μm and an output coupler fiber Bragg grating (OC FBG) with a core/cladding diameter of 30/400 μm are used to match the active fiber. The TMI thresholds of the lasers were 860 W and 1350 W when pumped by LDs with a central wavelength of 976 nm and 915 nm, respectively; these values were lower than those of a CCAF with a core/cladding diameter of 20/400 μm under the same conditions. A laser output of 1.7 kW was achieved when pumped with 915 nm LDs, as shown in Figure 8a. However, due to the immaturity of the fiber manufacturing process and the mismatch between the devices, the beam quality of the output laser at the maximum output power is about M^2 = 2.1, as shown in Figure 8b.

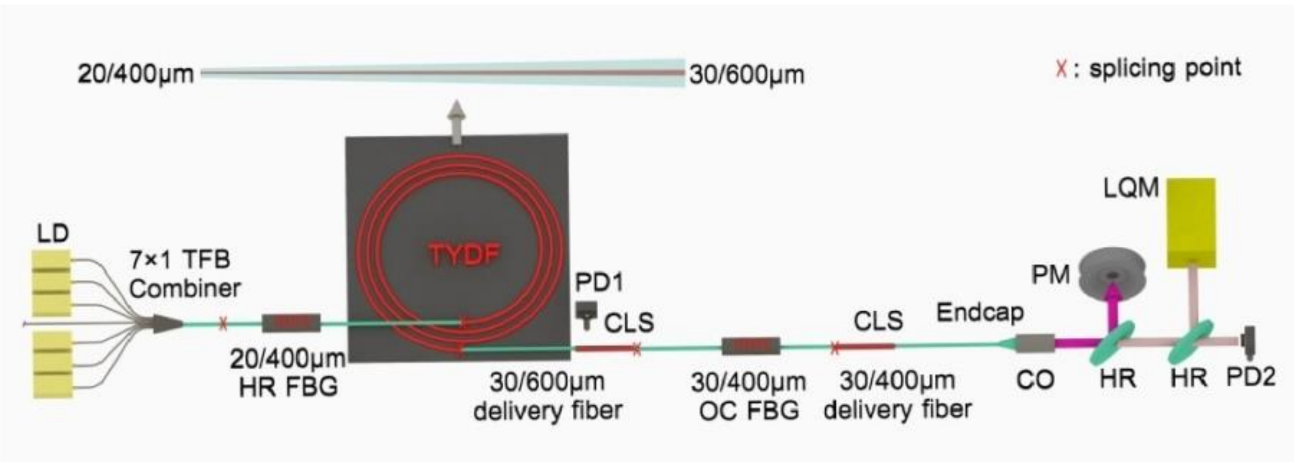

Figure 7. TF-based all-fiber laser oscillator. Reprinted with permission from Ref. [84], copyright 2019, Optical Society of America.

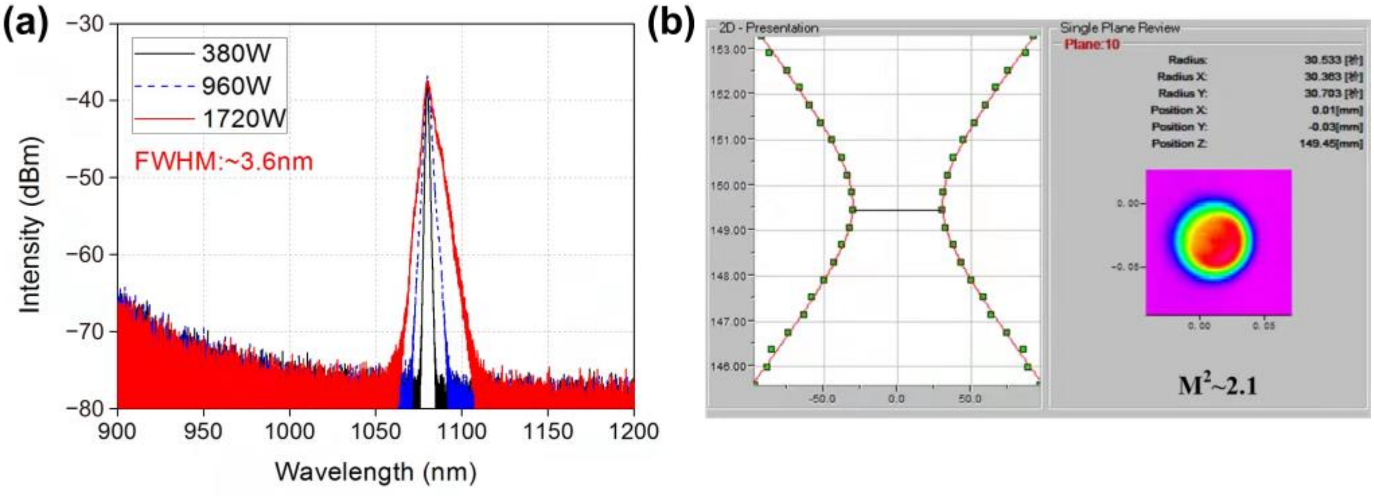

Figure 8. Output results of the TF-based fiber laser oscillator. (**a**) Spectra at different output powers; (**b**) beam quality at the maximum power. Reprinted with permission from ref. [84], copyright 2019, Optical Society of America.

4.1.2. High-Power Fiber Laser Amplifier Based on TF-CCCR

(1) Comparison study of the fiber laser amplifier employing TF-CCCR and CCAF

The results in the fiber laser oscillator show that the TMI threshold of a TF-based fiber laser is lower than that of a CCAF with a core diameter consistent with its S section. However, for a more reasonable comparison of the TMI thresholds of CCAF and TF, an active fiber with the same doping and equivalent core diameter should be selected. In 2019, we conducted experiments comparing the output characteristic of CCAF and TF-CCCR-based fiber laser amplifiers [85]. The structure of the laser is shown in Figure 9. The total length of the TF used is 22 m. The core/cladding diameter gradually transitions from 20/400 µm to 30/600 µm with the core/cladding NA of 0.065/0.46, respectively. The CCAF used for comparison has a core/cladding diameter of 25/400 µm, and its doping status and core/cladding NA remain the same as that of the TF-CCCR. A comparison of the experimental results is given in Figure 10 and Table 5. The maximum output power of the TF-CCCR-based amplifier is 2170 W, corresponding to an efficiency and beam quality (M^2 factor) of 79.1% and 2.2, respectively. The results successfully verified that the TMI threshold of TF-CCCR is higher than that of CCAF with the same equivalent core diameter. At the same time, it has better beam quality.

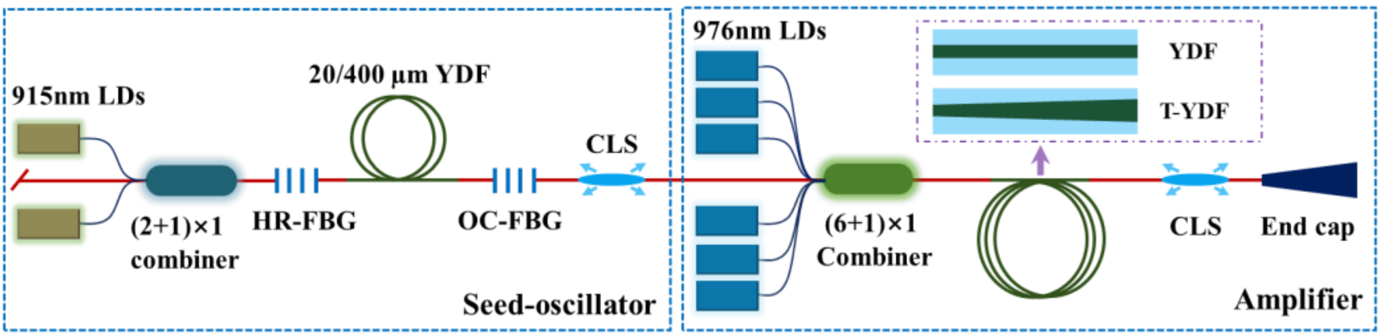

Figure 9. Schematic diagram of the experimental structure of the comparative experiment of fiber laser amplifiers based on CCAF and TF.

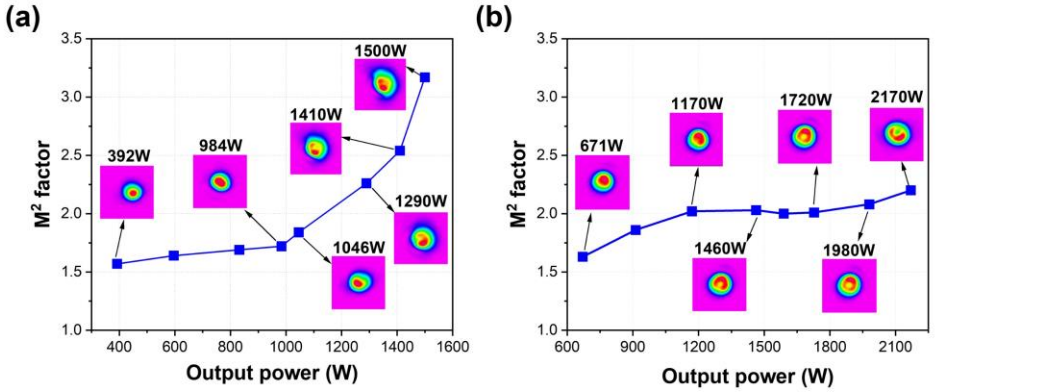

Figure 10. Comparison of experimental results of fiber laser amplifiers based on CCAF and TF. (**a**) The beam quality under different output powers when using 25/400 µm CCAF. (**b**) The beam quality under different output powers when TF-CCCR is applied [85].

Table 5. Comparison of results between TF-CCCR- and CCAF-based fiber laser amplifier [85].

Fiber	TMI Threshold	Efficiency	M^2
TF-CCCR	>2170 W	79.1%	2.2
CCAF (25/400 µm)	1046 W	80.3%	3.2

(2) Four-kilowatt near-single-mode fiber laser amplifier employing TF-CCCR

In 2022, we conducted experiments on bidirectionally pumped TF-CCCR-based laser amplifiers by combining a backward pump/signal combiner, which has a pump output fiber with a core/cladding diameter of 30/600 µm [95]. The experimental structure is shown in Figure 11. The total length of the TF-CCCR used is 17 m, and its core/cladding diameter gradually transitions from 20/400 µm to 30/600 µm. Distinct from the TF-CCCR used in the previous experiments, the distribution of the core diameter along the longitudinal direction of this TF-CCCR is approximately parabolic (concave), as shown in Figure 11b. According to the Ref. [102], such a structure has better mode control capability, which is advantageous for TMI suppression as well as beam quality enhancement. Due to the special characteristics of the fiber structure, the TMI threshold of the laser under co-pump configuration is higher than that in the counter-pump configuration. By reducing the coiling diameter of the L section of the fiber in the experiment, the efficiency is slightly reduced, and the beam quality is improved. A near-single-mode laser output of 4.09 kW with a slope efficiency of 84.1% and a beam quality of M^2~1.46 was achieved under bidirectional pump configuration at a coiling diameter of 12 cm for the large-size end, as shown in Figure 12.

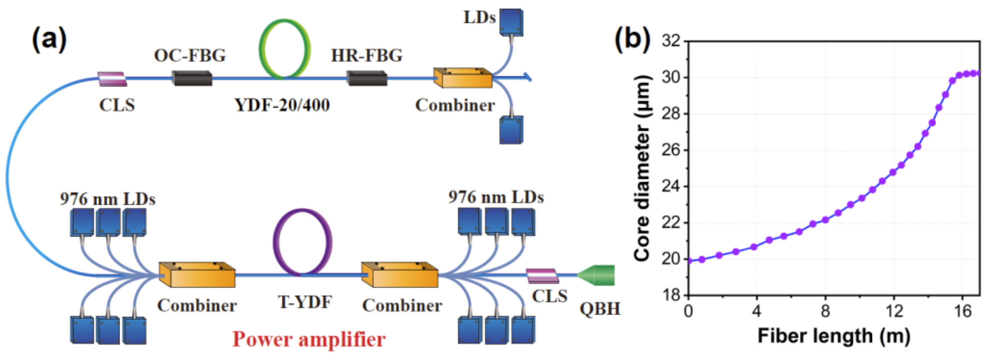

Figure 11. Schematic diagram of the experimental structure of the bidirectionally pumped TF-CCCR-based laser amplifier (**a**); and the distribution curve of core diameter along the longitudinal direction of the fiber (**b**). Reprinted with permission from Ref. [95], copyright 2022, Optica Publishing Group.

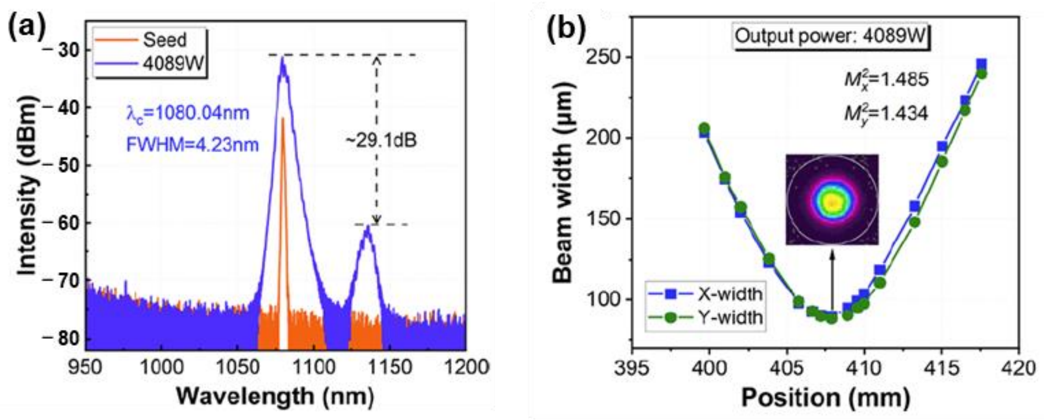

Figure 12. Experimental results of the bidirectional pumped TF-CCCR-based fiber laser amplifier. (**a**) The spectrum of the seed and the laser at the maximum output power. (**b**) The beam quality at maximum output power. Reprinted with permission from Ref. [95], copyright 2022, Optica Publishing Group.

(3) Six-kilowatt counter-pumped fiber laser amplifier employing TF-CCCR

Based on previous experiments, we optimized the structural parameters of the TF-CCCR and obtained a TF-CCCR with a total length of about 35.4 m (including 30 m in the T section and 5.4 m in the L section). The core/cladding diameters at both ends of the fiber are 20/400 µm and 30/600 µm, respectively. A counter-pumped fiber laser amplifier is constructed with 36 wavelength-stabilized 981 nm LDs and a (36 + 1) × 1 backward pump/signal combiner of which the core/cladding diameter is 30/600 µm for the signal input fiber [14]. As shown in Figure 13, the maximum output power of the laser is about 6110 W, corresponding to a slope efficiency of about 81.3%. No SRS appears in the spectrum at the maximum power, and the beam quality of the laser degrades to ~2.57. In fact, during the experiment, when the output power reaches about 5 kW, the time domain signal shows that the TMI has appeared in the laser, but the output power can continue to increase. As far as we know, this is the maximum power of the direct LD pumped fiber laser amplifier employing TF.

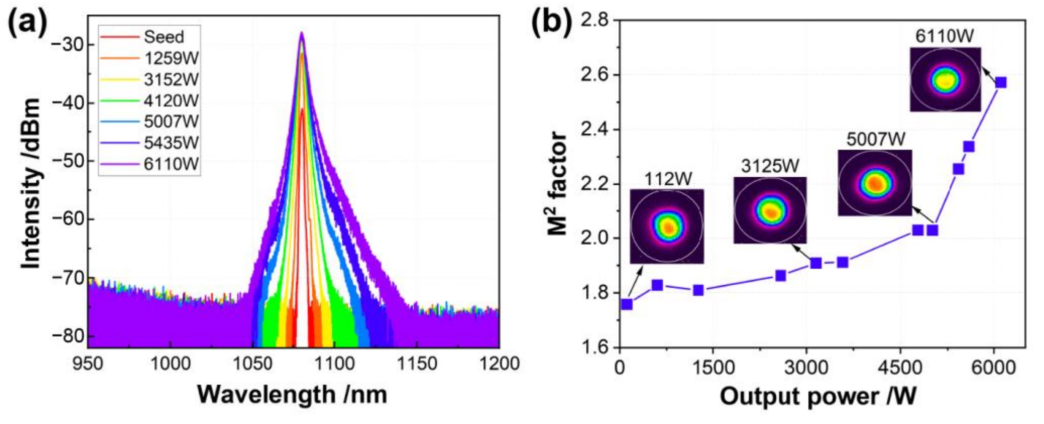

Figure 13. Results of the counter-pumped fiber laser amplifier based on TF-CCCR. (**a**) The spectra under different powers. (**b**) The beam quality of the laser under different powers.

4.1.3. Summary

From the existing results, the advantages and potential of TF applied to high-power fiber lasers have been verified experimentally. From the perspective of laser structure, the experimental research of a TF-based fiber laser oscillator is relatively limited in comparison to that of the fiber laser amplifier at present. In 2019, the output power of the laser oscillator was only less than 2 kW, and there is no updated progress so far. In the fiber laser amplifier, the output power has exceeded 6 kW, and the power of near single-mode laser has also exceeded 4 kW. All TF used in our experiment are TF with a constant core-to-core ratio. In ref. [69], the amplifier based on TF with a constant cladding diameter (TF-CCD) was carried out, and good results were also obtained. According to the theoretical research of Section 3, TF-CCD may have greater potential. At present, the manufacturing processes of VCAF and fiber devices are relatively mature, and the high-power fiber laser oscillator based on TF is worth further research. The aim of the next development of a high-power fiber laser amplifier based on TF is to achieve higher power and better beam quality. These are achieved by optimizing the fiber and laser structure parameters (such as pump wavelength, fiber coiling, etc.).

4.2. Fiber Laser Based on SAF

4.2.1. Fiber Laser Oscillator Based on SAF with Tapered Core and Constant Cladding

Compared with the TF, the SAF has a more versatile longitudinal structure and also has the ability to accommodate both SRS and TMI. In 2020, we demonstrated the first experiment of an SAF-based fiber laser oscillator with an output power of more than 1 kW [71]. Different from the typical SAFs that can be divided into five sections along the longitudinal direction, this SAF, with a total length of 27 m, can be divided into three sections: two L sections (L1 and L2) at both ends and a saddle-shaped section (SA section) in the middle. The longitudinal core diameter distribution and main structural parameters of this SAF are shown in Figure 14 and Table 6. The results are shown in Figure 15. The TMI threshold of the laser is about 702 W when the pump wavelength is 976 nm, whereas it is higher than 1312 W when the pump wavelength is 915 nm. Due to the lack of maturity of the production process, the fiber has a more serious eccentricity (>7 μm), which leads to poor beam quality of the output laser (~2.0 @1312 W), low optical conversion efficiency (46%) and more serious melting-point heating phenomenon, which also has a greater impact on the TMI threshold and ultimately limits the further increase of the output power.

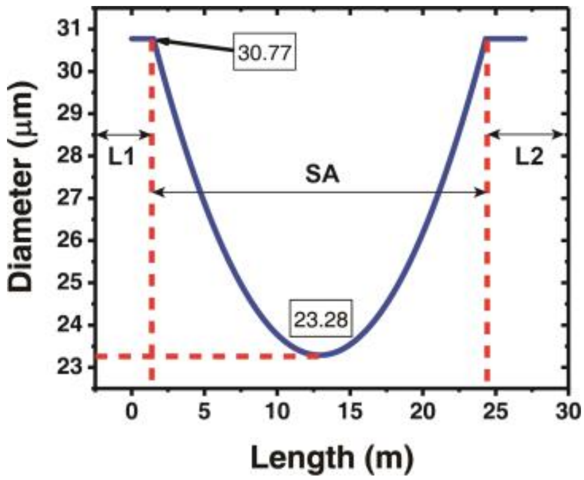

Figure 14. The core diameter of the SAF at different sections along the longitudinal direction.

Table 6. Fiber parameters in different sections.

Section	Core Diameter/μm	Cladding Diameter/μm	Length/m
L1	30.77	400	1.5
SA	30.77-23.28-30.77	400	22.8
L2	30.77	400	2.7

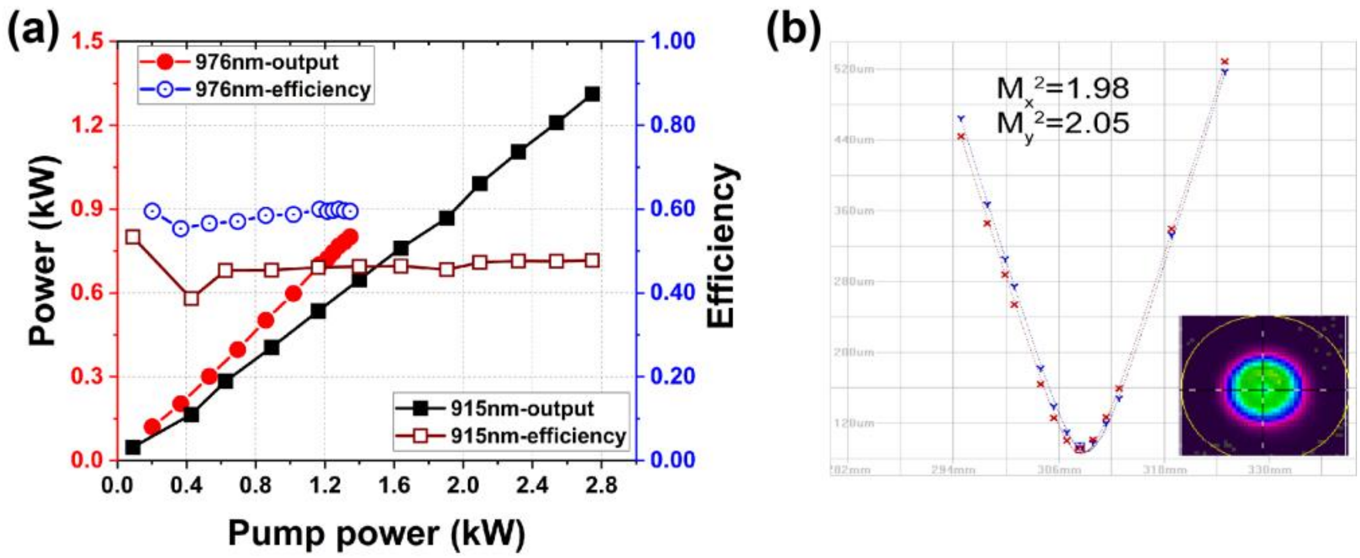

Figure 15. Experimental results of SAF-based laser oscillator. (**a**) The output power and efficiency at different pump powers when pumped by LDs with different wavelength. (**b**) The beam quality at output power of 1312 W [71].

4.2.2. Fiber Laser Amplifier Based on SAF with Tapered Core and Constant Cladding

In 2022, a high-power fiber laser amplifier were conducted based on a newly designed and fabricated SAF which aims for good beam quality [103]. The core diameter distribution of this fiber is similar to that of the fiber in Figure 14, and the corresponding parameters are shown in Table 7.

Table 7. Fiber parameters in different section of SAF used for fiber laser amplifier.

Section	Core Diameter/µm	Cladding Diameter/µm	Length/m
L1	30.0	600	1.0
SA	30.0-20.8-30.0	600	32.0
L2	30.0	600	1.0

The output characteristics of the laser are tested under the conditions of co- and counter-pump configurations with non-wavelength-stabilized 976 nm LDs. The experimental results are shown in Figure 16. The maximum power of the amplifier under co- and counter-pump configuration is ~1.8 kW and ~1.5 kW, respectively, and the corresponding TMI threshold is ~1797 W and ~1484 W. It is noteworthy that the output laser beam quality of the current laser is greatly improved compared to the aforementioned SAF-based laser oscillator (M^2~2.0). The beam quality of the output laser remained essentially below 1.4 before the advent of TMI. The results of this experiment show that the optimized design of the SAF can ensure good output laser beam quality while suppressing SRS in the laser. Currently, the TMI of the SAF-based fiber laser is the main limiting factor for power enhancement, and subsequent studies can improve the performance of the fiber from pump, fiber coiling, and fiber design.

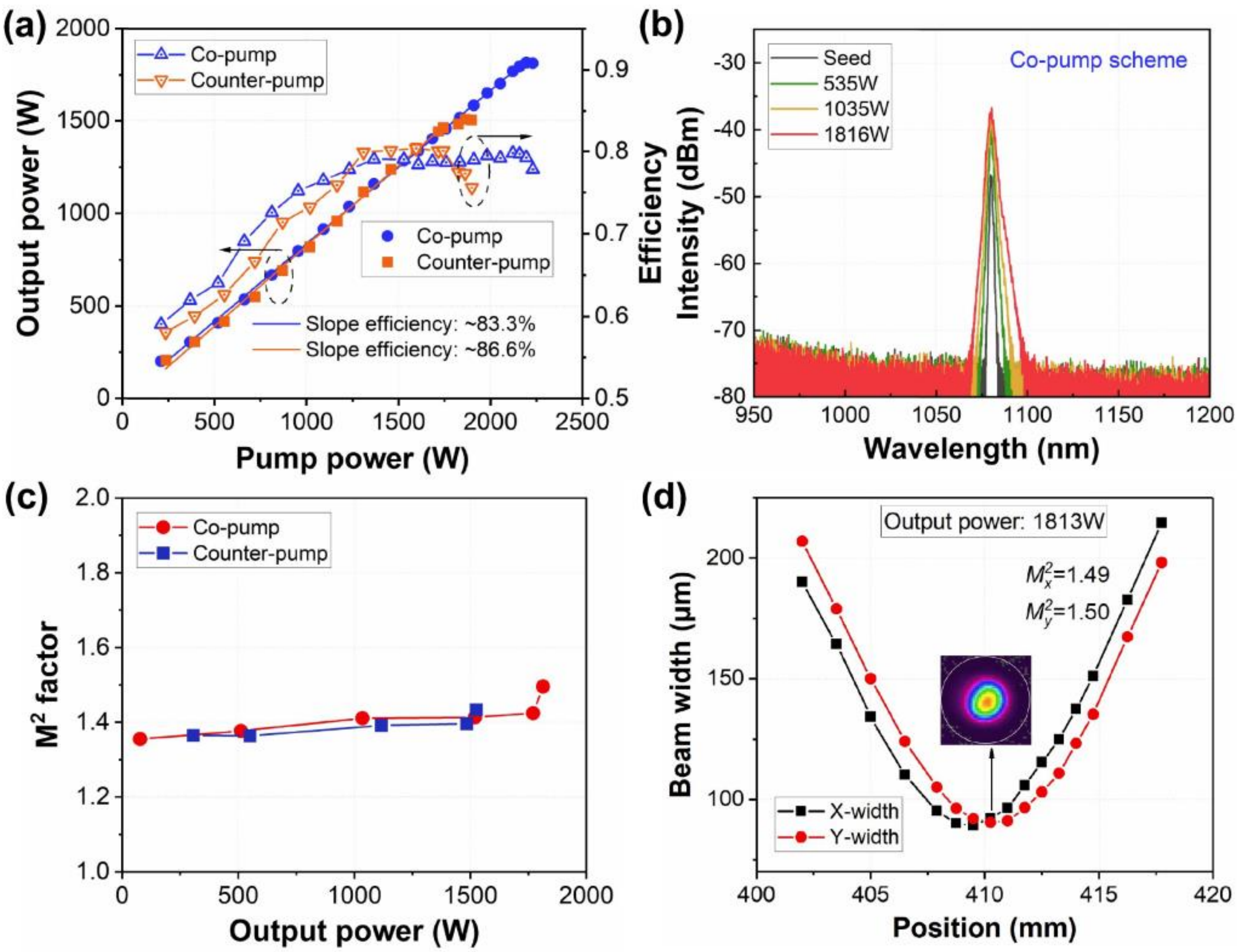

Figure 16. Output results of laser amplifier based on SAF. (**a**) The output laser power and efficiency at different pump powers for co- and counter-pump configurations; (**b**) the output spectrum under co-pump configuration; (**c**) the beam quality results at different output powers; (**d**) the beam quality measurements at an output of 1813 W under co-pump configuration [103].

4.2.3. Summary

The experimental research of fiber laser based on SAF is the most limited among several VCAF at present. At present, only a 1.3 kW fiber laser oscillator and a 1.8 kW fiber laser amplifier have been realized. In the 1.3 kW SAF-based fiber laser oscillator, the im-mature fiber technology leads to the poor beam quality of the output laser and the difficulty of fiber-fusion processing. These factors limit the improvement of output power and laser beam quality. In the 1.8 kW fiber laser amplifier, the problems of fiber technology have been basically solved, and the laser has the potential to achieve more than 3 kW laser output by bidirectional pump. Therefore, an SAF-based fiber laser has been able to achieve high efficiency and high beam quality laser output. Combined with the optimization of fiber parameters (core diameter distribution, cladding diameter, length distribution, doping, etc.), several kW fiber laser amplifiers and oscillators with high beam quality can be realized in the future. In addition, the current research involves SAF with tapered core and constant cladding, and the realization of high-power laser output based on SAF with a constant core-to-cladding ratio is also worth further exploration.

4.3. Fiber Laser Based on SPF

4.3.1. Fiber Laser Employing SPF with Constant Core-to-Cladding Ratio (SPF-CCCR)

(1) Fiber laser (3–5 kW) employing SPF-CCCR

Different from SAF, the S1 section and the S2 section at the two ends of the SPF have better mode control capability, which is more advantageous for achieving high beam quality fiber lasers. In 2020, we conducted the first experiments with a fiber laser oscillator based on a self-designed SPF-CCCR [70]. The total length of the fiber is 30.9 m, and its longitudinal structure is shown in Figure 17. The fiber is fabricated using the variable-speed drawing method described in Section 2.3.2 with a constant core-to-cladding ratio, and the cladding pump absorption coefficient is comparable to the commercial 20/400 µm CCAF. Under the condition of a bidirectional pump with wavelength-stabilized 976 nm LDs, we finally achieved a 3 kW near-single-mode laser output with beam quality M^2~1.3 and an optical-to-optical conversion efficiency of 78.4%. Figure 18 shows the output spectrum and beam quality of the laser. Compared with lasers based on CCAF with core/cladding diameters of 21/400 µm (see Table 8), this laser has better SRS suppression while maintaining good beam quality [104].

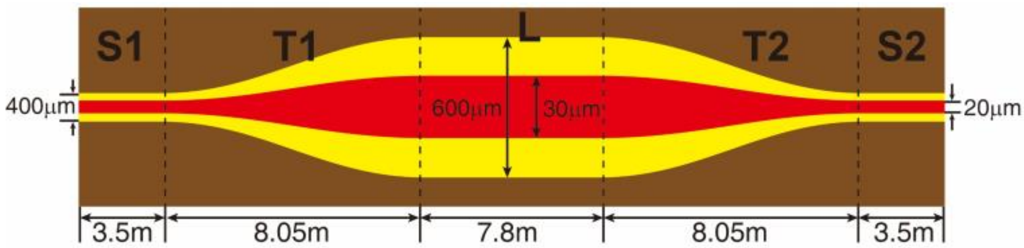

Figure 17. The longitudinal structure of the SPF. Reprinted with permission from Ref. [70], copyright 2020, Optical Society of America.

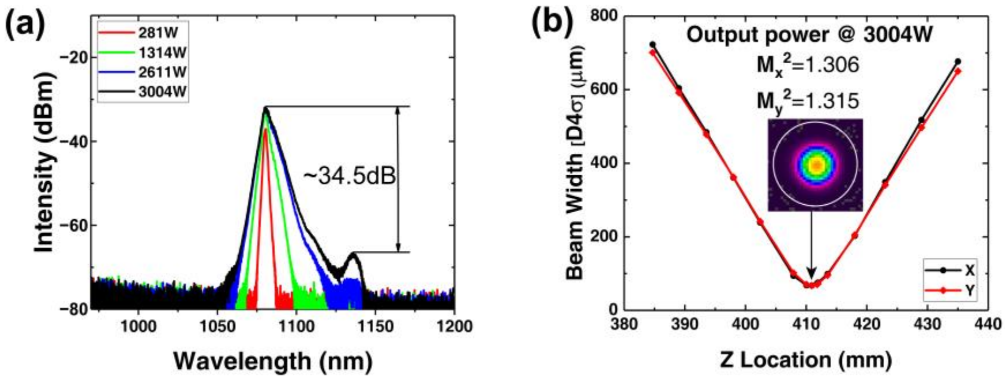

Figure 18. Experimental results of the SPF-based fiber laser oscillator. (**a**) The measured spectra at different output powers. (**b**) The measured M^2 at the maximum output power. Inset: a beam profile of the output laser. Reprinted with permission from Ref. [70], copyright 2020, Optical Society of America.

Table 8. Comparison of the main results of 3 kW near single-mode fiber laser oscillator based on SPF [70] and CCAF [104].

Fiber Type	Pump Wavelength/Configuration	Maximum Power	TMI	Fiber Length	SRS	Efficiency	M^2
21/400 µm CCAF	976 nm /bidirectional	3050 W	>3050 W	18 m	−29 dB	73%	~1.3
SPF	976 nm /bidirectional	3004 W	>3004 W	30.9 m	−34 dB	78%	~1.3

In the above fiber laser oscillator, due to the long fiber length, a significant SRS is already present in the spectrum at the maximum output power and limits the further power scaling. To suppress SRS, a strategy can be adopted to design SPF with larger core diameters. In 2021, we designed an SPF-CCCR with core/cladding diameter distribution of 25/400 μm–37.5/600 μm–25/400 μm, based on the above SPF-CCCR. As shown in Figure 19, the fiber was applied to a fiber laser amplifier, and a laser output of 5 kW was finally achieved, which has good SRS suppression [92]. However, the output laser beam quality of this laser is about 1.9 because of fiber fusion as well as devices.

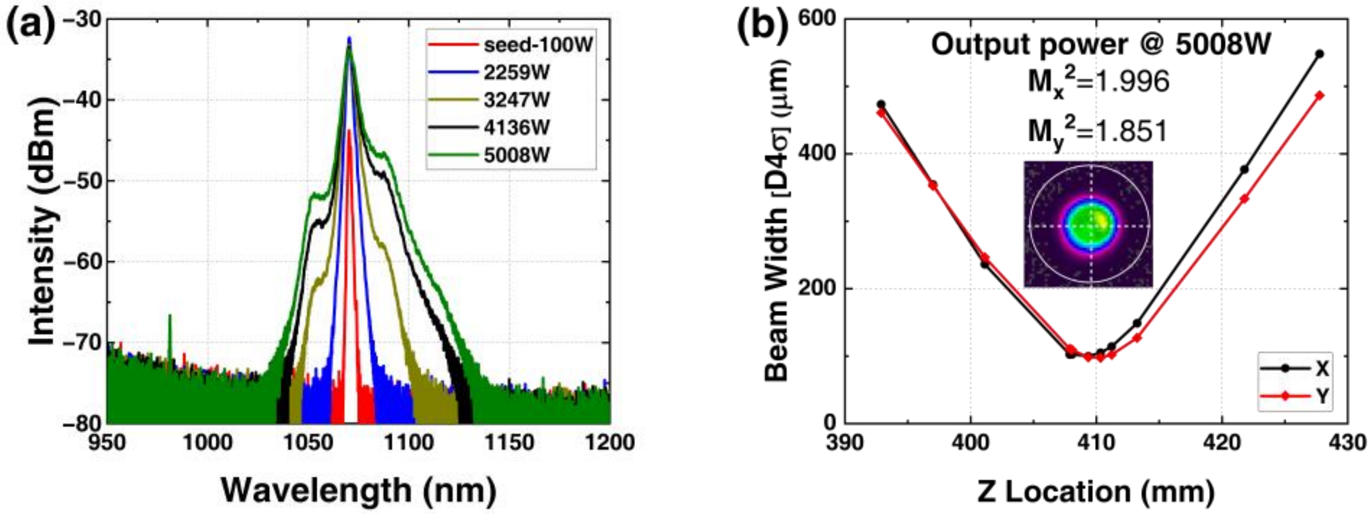

Figure 19. Output results of a fiber laser amplifier based on an SPF-CCCR. (**a**) Output spectra at different output powers. (**b**) Beam quality at the maximum output power. Reprinted with permission from Ref. [92], copyright 2021, Optical Society of America.

(2) 6 kW fiber amplifier employing SPF-CCCR

In 2022, we increased the output power of a fiber laser amplifier based on an SPF-CCCR to 6 kW. The self-designed and fabricated SPF-CCCR has a total length of 30 m. The core diameter distribution is 25/400 μm–37.5/600 μm–25/400 μm, which is the same as that of the SPF-CCCR in the 5 kW fiber laser amplifier described above. The pump source of the amplifier is a series of wavelength-stabilized LDs with a central wavelength of 981 nm, and the pump absorption coefficient of the SPF-CCCR is 0.81 dB/m @981 nm. When the unidirectional pump configuration is applied, the maximum output power achieved in the co- and counter-pump configurations is 2780 W and 4307 W, respectively. Moreover, neither TMI nor SRS is present at the maximum power, and the power scaling under unidirectional pump is limited by the pump power. When applying bidirectional pump configuration, an output power of 6020 W was obtained at a co- and counter-pump power of 2417 W and 5263 W, respectively. No TMI was observed at the maximum output power, and the SRS intensity was about 26.7 dB lower than the signal. The beam quality measurements and beam profile at the maximum output power are shown in Figure 20d, with the value of $M_x^2 = 1.87, M_y^2 = 1.85$.

4.3.2. Fiber Laser Based on SPF with Constant Cladding Diameter (SPF-CCD)

From the process of fabrication, SPF-CCCR is made mainly by a variable-speed drawing method. The production process of preform is simple, but the drawing speed is not easy to control precisely, and the fiber coating is more difficult, especially when the diameter difference between the L section and the S section is relatively large. The preform form control method can be used to manufacture VCAF with a constant cladding diameter. The coating process of such fibers is relatively easy, and the drawing speed of the manufacturing process does not need to be changed. In addition, the cladding pump absorption coefficient of a VCAF with a constant cladding diameter gradually changes, resulting in a more uniform heat distribution in the fiber, which is more conducive to TMI suppression (as shown in the simulation results in Section 2).

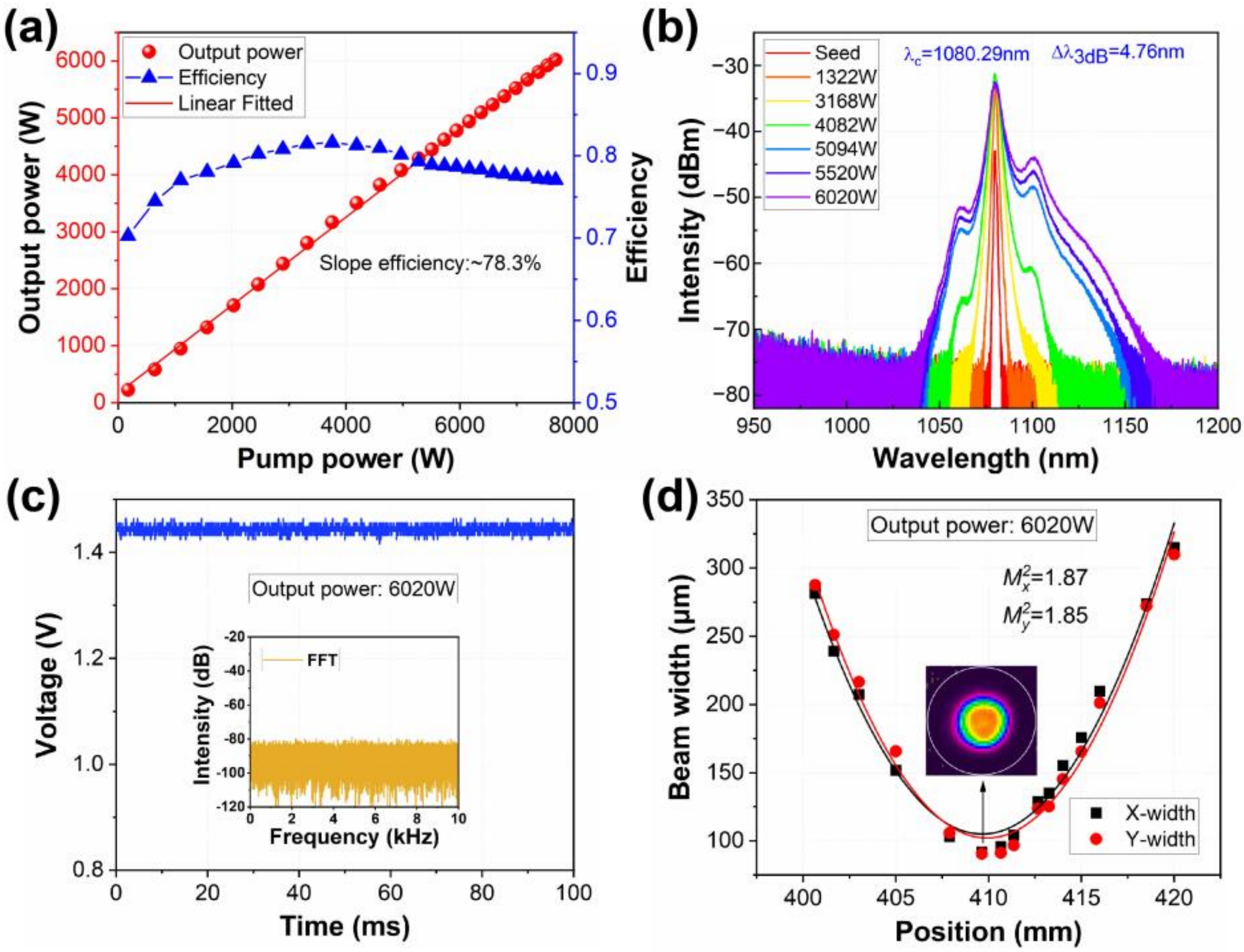

Figure 20. Experimental results of 6 kW SPF-CCCR based fiber laser amplifier. (**a**) Output laser power and efficiency at different pump powers. (**b**) Output spectra at different output powers. (**c**) PD signal at the maximum output power and its corresponding FFT results. (**d**) Beam quality results at the maximum output power (inset: the beam profile of the laser).

In 2021, we conducted the first high-power fiber laser oscillator based on an SPF-CCD [72]. The refractive index distribution within the cross-section of the fiber and the distribution curve of the core diameter along the longitudinal direction are shown in Figure 21. The total length of the fiber is 25 m. In contrast to the structure of a typical SPF, as shown in Figure 1b, there is no S section at either end. The core diameter in the middle L section is 31 μm, and the length is 4.8 m; the minimum core diameter of the two T sections at both ends is 24.1 μm and 23.4 μm, respectively, and the length is 10.1 m. The core NA along the longitudinal direction remains constant at ~0.065. According to the theoretical results, the core diameter variation curve in the T section of the fiber is designed as a concave function, approximating a parabola, for the best mode control ability and TMI suppression. The output spectrum and beam quality of the laser are shown in Figure 22. The fiber laser oscillator with bidirectional pump structure was measured to have a TMI threshold of ~3.12 kW, and the maximum output power of the laser was 3420 W. No SRS appeared on the spectrum, and before the appearance of TMI, the beam quality of the laser was about 1.7.

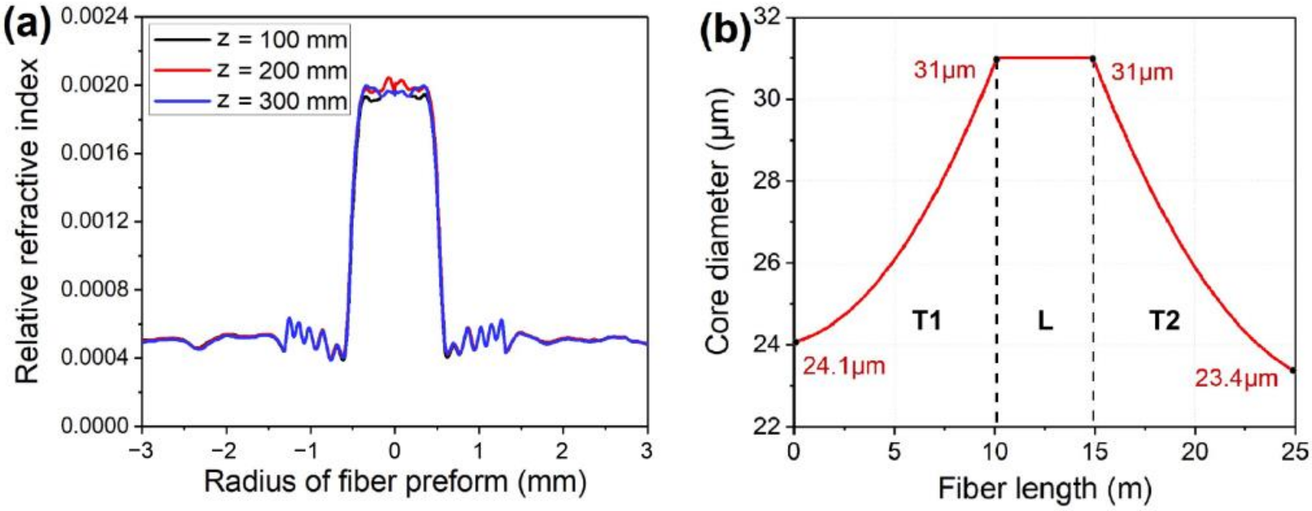

Figure 21. (**a**) Refractive index profile at different positions along the length of the preform; and (**b**) the core diameter distribution of the fabricated SPF-CCD [72].

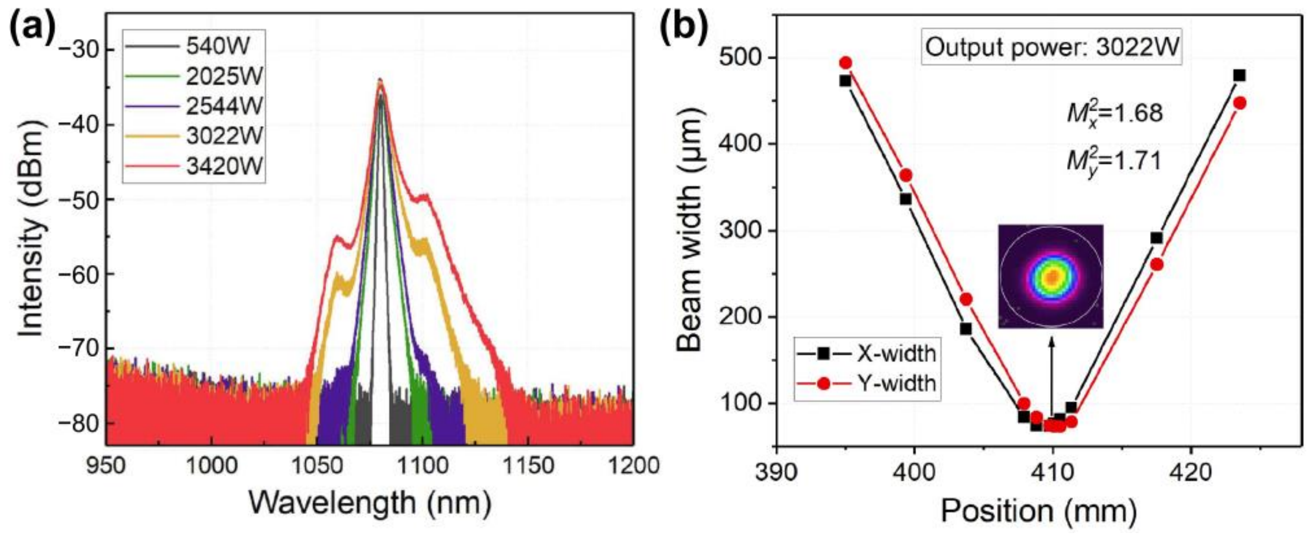

Figure 22. Output results of an oscillator based on an SPF-CCD. (**a**) The spectra at different output powers. (**b**) The beam quality of the laser at a power of 3 kW [72].

4.3.3. Comparison of SRS of Fiber Laser Amplifier Based on SPF-CCCR and CCAF

Based on the aforementioned 6 kW amplifier in 4.3.1, the SPF-CCCR in the amplifier stage is replaced by a CCAF with a core/cladding diameter of 25/400 μm. This fiber is made from the same fiber preform as the adopted SPF-CCCR with identical core doping and NA parameters. Comparing the results, there is no TMI in both unidirectional and bidirectional pump conditions when two fibers are used. At an output power of 6 kW, the beam quality of the two is basically at the same level. However, the beam quality values are slightly worse for the SPF-CCCR due to the fiber matching, as shown in Figure 23a,b. Significant SRS is observed with the CCAF, whereas SRS is ~3 dB better suppressed with the SPF-CCCR, as shown in Figure 23c.

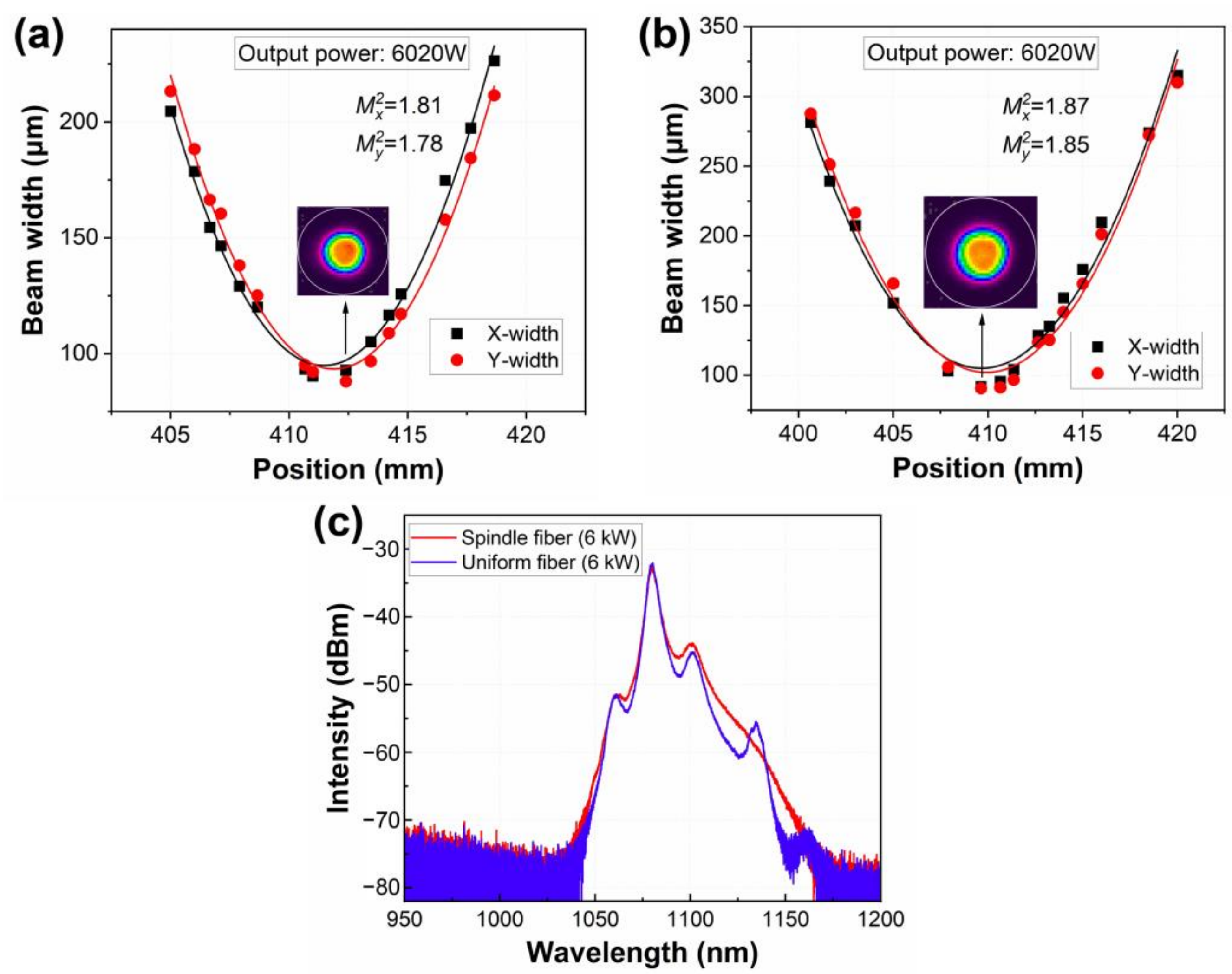

Figure 23. Comparison of experimental results between SPF-CCCR and 25/400 μm CCAF under the same conditions. (**a**) The beam quality of the output laser with CCAF. (**b**) The beam quality of the output laser with SPF-CCCR. (**c**) Comparison of the spectra of the two fibers at the same output power (6 kW).

4.3.4. Comparison of TMI of Fiber Laser Amplifier Based on SPF-CCD and CCAF

Theoretical analysis shows that SPF are capable of accommodating both SRS and TMI in fibers. The theoretical study in Section 3 shows that the suppression of SRS is close to that of a conventional fiber with the same equivalent core diameter, but the VCAF has a higher TMI threshold. In 2022, we experimentally and rigorously compared TMI in CCAF and SPF-based amplifiers [73]. The SPF-CCD (named CCTC fiber in ref. [73]) and CCAF used for comparison are both from the same preform, which can avoid experimental errors due to differences in fiber properties. The SPF-CCD is similar to the VCAF in [72]. The core and cladding diameters of the CCAF are 28 μm and 600 μm, respectively, corresponding to the equivalent core and cladding diameters of the SPF-CCD. The key parameters of the two fibers are shown in Table 9. All experimental conditions, including pump source, fiber devices, and fiber coiling diameter, were kept consistent.

The results are shown in Figure 24, the TMI thresholds of CCAF-based fiber laser amplifier in both the co- and counter-pump are 1135 W and 2056 W. However, the TMI thresholds of the SPF-CCD-based fiber laser amplifier in both the co- and counter-pump are 1324 W and 2494 W. The results show that the SPF-CCD-based fiber laser amplifier has a higher TMI threshold in both co- and counter-pump configurations. Throughout the experiment, the beam quality of the SPF-CCD-based fiber laser amplifier remains near 1.3, whereas the beam quality of the uniform size fiber is always above 1.4 and degrades gradually.

Table 9. Fiber parameters of SPF-CCD and CCAF. Adapted with permission from Ref. [73], copyright 2022, Optica Publishing Group.

Fiber Type	Core/Cladding Diameter	Core NA	Average Absorption Coefficient	Length
SPF-CCD	20-36-20/600 µm	0.065	0.78 dB/m	28.5 m (11.1 m-6 m-11.4 m)
CCAF	28/600 µm	0.065	0.80 dB/m	27.8 m

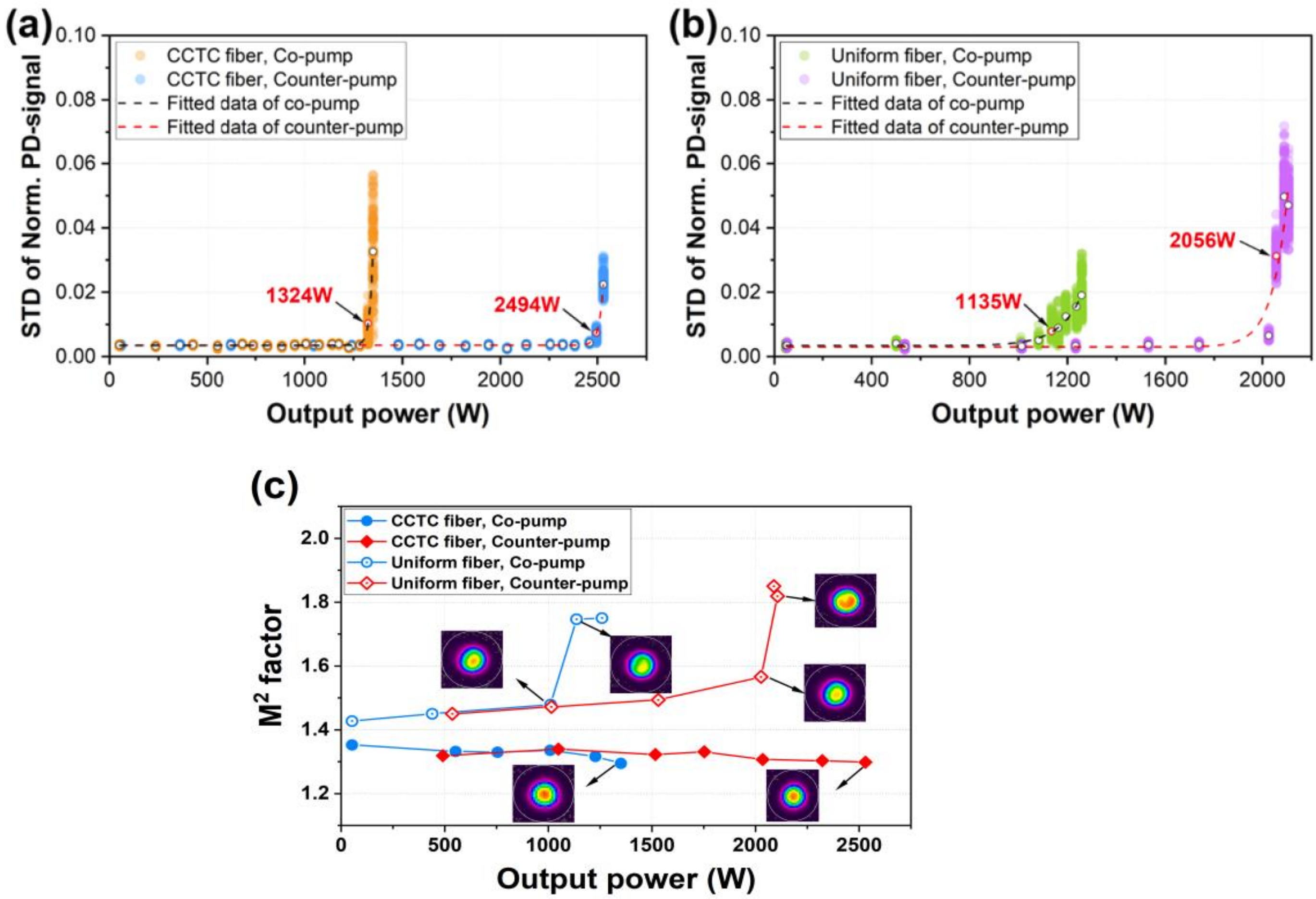

Figure 24. (**a**) The STD of the normalized PD-signal of the SPF-CCD (CCTC) fiber amplifier under co-pump and counter-pump schemes. (**b**) The STD of the normalized PD-signal of the CCAF amplifier under co-pump and counter-pump schemes. (**c**) The beam quality evolution during the power scaling of both fiber amplifiers. Reprinted with permission from Ref. [73], copyright 2022, Optica Publishing Group.

4.3.5. Summary

In general, because the fiber laser based on SPF is the first VCAF to realize several kilowatts of near-single-mode laser output, it has received more attention and been subjected to more research. The work described above is based on the wide-linewidth CW high-power fiber laser developed by SPF. At present, the maximum output power of the oscillator has reached 3420 W, and the output power of the fiber laser amplifier has exceeded 6 kW. The balance advantage of SPF for SRS and TMI has also been verified experimentally. The next research direction is to achieve higher power laser output and improve beam quality by optimizing fiber parameters and laser structure. In addition to the above results, SPF has also been applied to narrow linewidth fiber lasers at present, and 4.18 kW near-single-mode narrow linewidth laser output has been achieved. The combination of SPF and confined-doped, low NA and other measures shows the great potential of VCAF in the field of high-power fiber lasers.

5. Application of VCAF in Novel Fiber Lasers

5.1. Quasi-Continuous Wave Fiber Laser Based on TF and SPF

In addition to the conventional CW fiber lasers mentioned above, VCAF have great potential in QCW fiber lasers, which have repetition frequencies in the range of kHz and exhibit a pulsed state with low average power and high peak power. As a result, QCW fiber lasers tend to be limited by nonlinear effects rather than TMI, especially SRS. The application of VCAF to QCW fiber lasers can fully utilize its good beam quality retention and SRS suppression capability.

5.1.1. Peak Power of 6.4 kW for QCW Fiber Laser Based on TF-CCCR

Firstly, QCW fiber lasers based on TF-CCCR have also been conducted. The total length of the fiber is 17 m, and the core/cladding diameter varies linearly from 20/400 µm to 30/600 µm. Moreover, the absorption coefficient is ~0.4 dB@915 nm. The structure of the optical part of the laser is shown in Figure 25. Combined with a (36 + 1) × 1 backward pump/signal combiner with better performance, the laser is purely counter-pumped, which ensures the best SRS suppression. The combiner is placed inside the resonant cavity to achieve the best fiber matching. At a total average pump power of 915 W, a laser output with an average power of 646 W with a conversion efficiency of 70.6% was obtained, corresponding to a peak power of 6.42 kW. The spectrum and beam quality of the output laser are shown in Figure 26c,d, with the beam quality M^2~1.60. The SRS intensity is 19.8 dB lower than the signal.

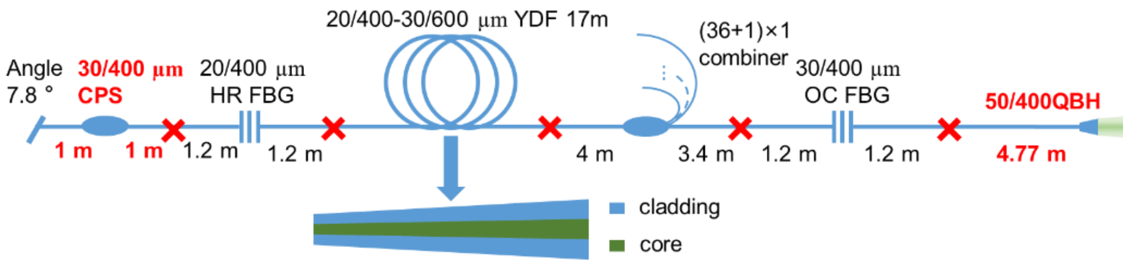

Figure 25. Schematic diagram of the optical part of a QCW fiber laser based on a TF-CCCR.

5.1.2. Peak Power of 7.3 kW for QCW Fiber Laser Based on SPF-CCCR

Then, in order to improve the beam quality and output power, we used an SPF-CCCR in the QCW fiber laser, and a peak power of 7.3 kW was achieved [97]. As shown in Figure 27, the core diameter distribution of the SPF-CCCR used is 25/400 µm–37.5/600 µm–25/400 µm, with a total length of 24 m and a length distribution of 2 m–6 m–8 m–6 m–2 m, and the equivalent core diameter of the fiber is 32.6 µm. Based on this fiber, combined with the optimization of the OCFBG, a QCW with a peak power of 7.3 kW was achieved at a co-/counter-pump power ratio of 1:9.2 and a total average pump power of 853 W. The efficiency of the laser was about 67%, the beam quality M^2 factor is about 1.43, and the intensity of SRS is 26 dB lower than the signal. The spectra in Figure 28a show that a small amount of co-pump power leads to a rapid increase in SRS in the output laser, but the control system of the pump source is limited by the inability to achieve a further increase in the proportion of backward pumping.

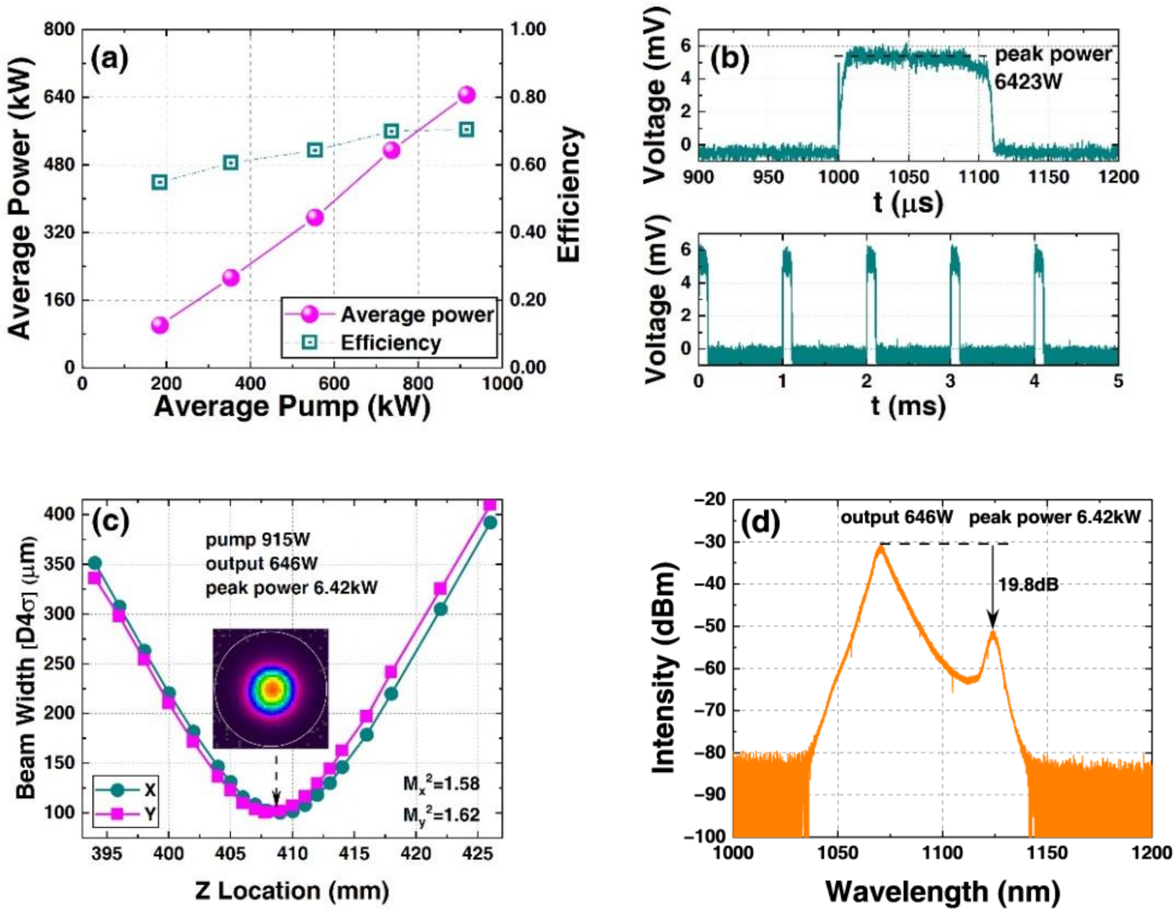

Figure 26. Output results of QCW fiber laser based on TF-CCCR. (**a**) The average output power and efficiency at different average pump powers. (**b**) The time-domain pulse profile at peak power of 6423 W. (**c**) The beam quality and beam profile at the maximum output power. (**d**) The output spectrum at the maximum power.

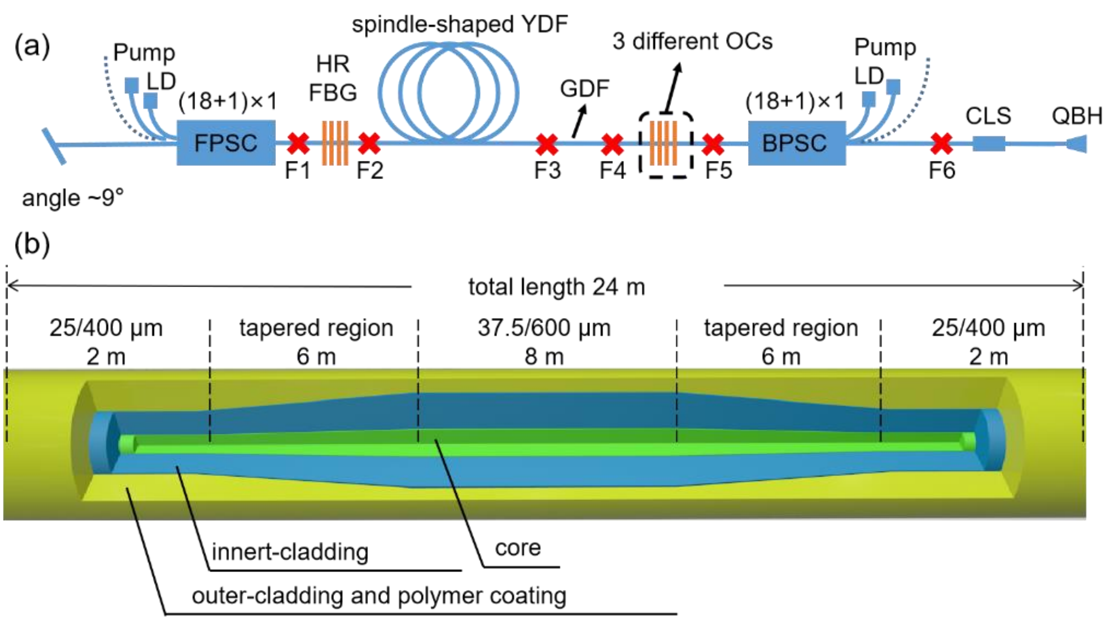

Figure 27. Schematic diagram of the structure of a QCW fiber laser based on SPF-CCCR (**a**) and the longitudinal structure of the SPF-CCCR (**b**) [96].

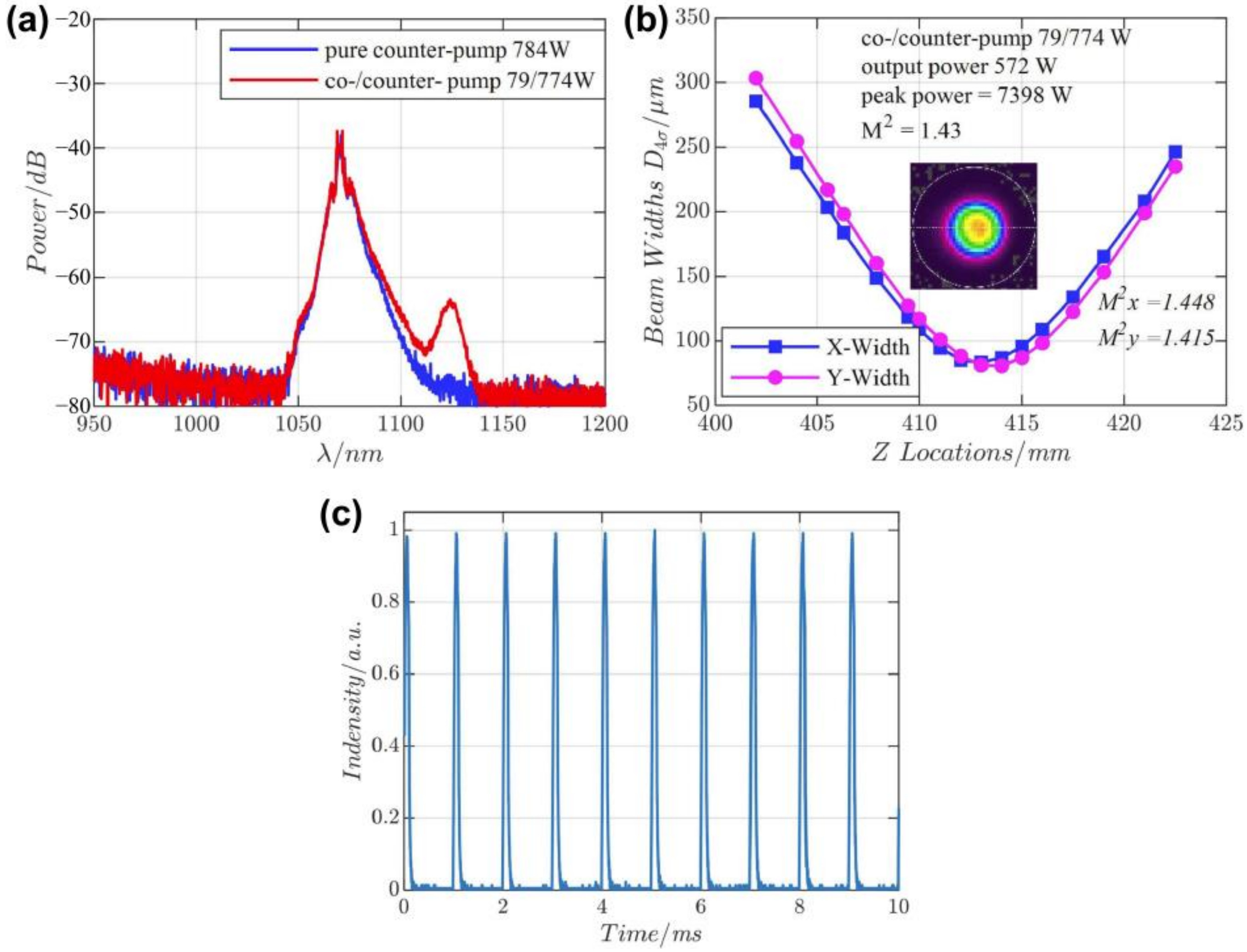

Figure 28. The main output results of the QCW fiber laser. (**a**) The output spectrum at the maximum power under different pump configurations. (**b**) The beam quality and beam profile at the maximum output power. (**c**) The time-domain pulse profile at peak power of 7398 W [97].

The recently main results of QCW fiber laser oscillators based on CCAF and VCAF are listed in Table 10 [105]. It can be found that the significant advantage of VCAF is the good mode control capability for achieving near single-mode QCW fiber laser, but the current VCAF is either too long or the equivalent core diameter is small, which does not fully exploit its advantages. Considering that the TMI threshold is much higher than the SRS threshold in QCW fiber lasers, VCAF for QCW fiber lasers should have a larger equivalent core diameter and a shorter fiber length.

Table 10. Comparison of the main results of QCW fiber lasers based on CCAF and VCAF [96,97,105].

Fiber Type	Fiber Length	Equivalent Core Diameter	Bandwidth (HR/OC)	Pump Configuration	Peak Power	Efficiency	SRS	M^2
30/400 CCAF	15 m	30 μm	4.05/2.05 nm	Bidirectional	9713 W	61.6%	>24 dB	2.40
TF-CCCR	17 m	25 μm	3.05/1.98 nm	Counter	6420 W	70.6%	19.8 dB	1.60
SPF-CCCR	24 m	32.6 μm	4.09/1.01 nm	Bidirectional (1:9.2)	7398 W	67.0%	26 dB	1.43

5.2. Optimization of Output Characteristics of Oscillating–Amplifying Integrated Fiber Laser Employing SPF-CCCR

The oscillating–amplifying integrated fiber laser (OAIFL) is a new structure fiber laser that is distinct from the traditional fiber laser amplifier and the fiber laser oscillator. The OAIFL can combine the advantages of the latter two, including high efficiency, good anti-reflection capability, simple pump control logic, and compact structure. In 2021, we achieved for the first time an OAIFL at 5 kW power level based on a CCAF with a core/cladding diameter of 25/400 μm. In that study, severe SRS was observed when the output power exceeded 5 kW, whereas the laser operating state was already close to the TMI threshold, and the beam quality of the output laser showed rapid degradation [106].

In 2022, we applied our self-designed SPF-CCCR to an OAIFL for the first time and improved its output characteristics [77]. The structure of the laser and the SPF-CCCR used is shown in Figure 29a,b and the results are shown in Figure 30. The laser adopts a bidirectional pump structure, and the active fiber of its oscillating section is a 22/400 μm CCAF with a length of 4.32 m. The SPF-CCCR in the amplifying section has a core/cladding diameter distribution of 25/400 μm–37.5/600 μm–25/400 μm and length distribution of each section of 2 m–6 m–2 m–5 m–6 m. In order to better balance SRS and TMI, the fiber has a low absorption design with a pump absorption coefficient ~0.471 dB/m@915 nm. Based on this structure, the maximum output power of the laser was measured to be 2710 W under co-pump configuration, because it was limited by SRS, and 4755 W under counter-pump configuration, because it was limited by available pump power. A maximum laser output of 6060 W was obtained when bidirectional pump configuration was applied. When the output power was 6020 W, the beam quality (M^2 factor) of the output laser was ~1.77, and the SRS intensity was about 18.2 dB lower than the signal. To the best of our knowledge, this is the highest output power of OAIFL with good beam quality at present.

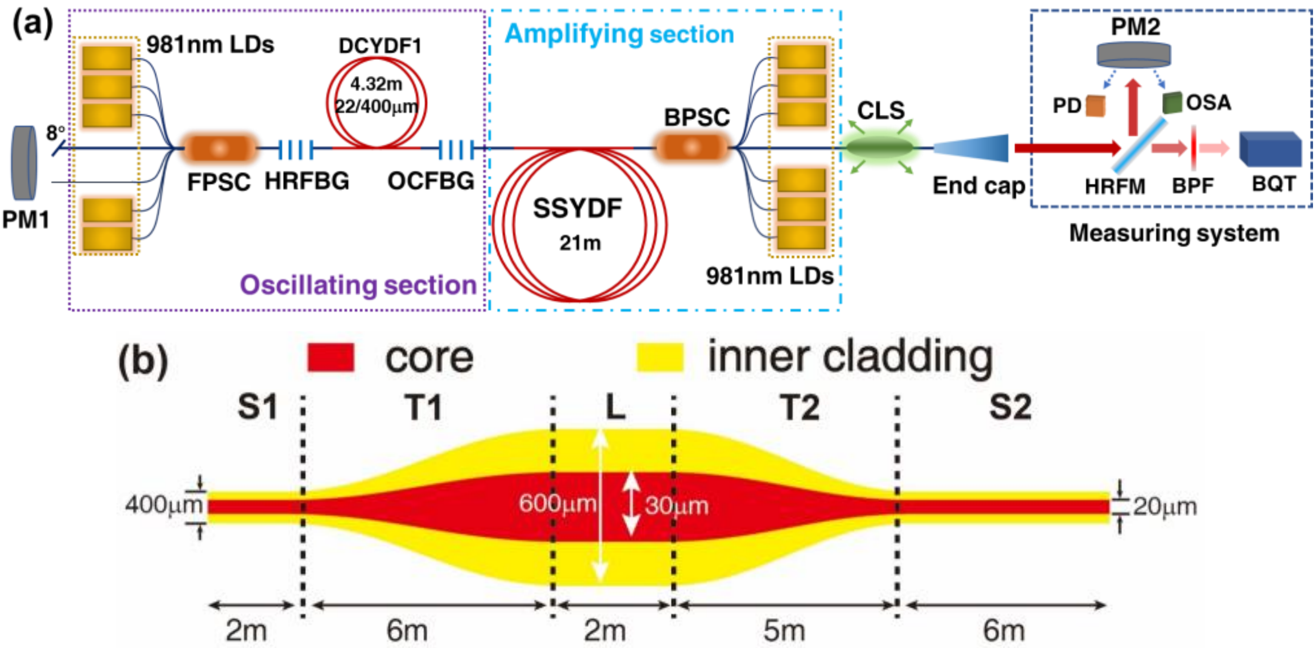

Figure 29. Schematic diagram of the structure of an oscillating–amplifying integrated fiber laser based on an SPF-CCCR. (**a**) Schematic diagram of the laser structure. (**b**) Schematic diagram of the SPF-CCCR [77].

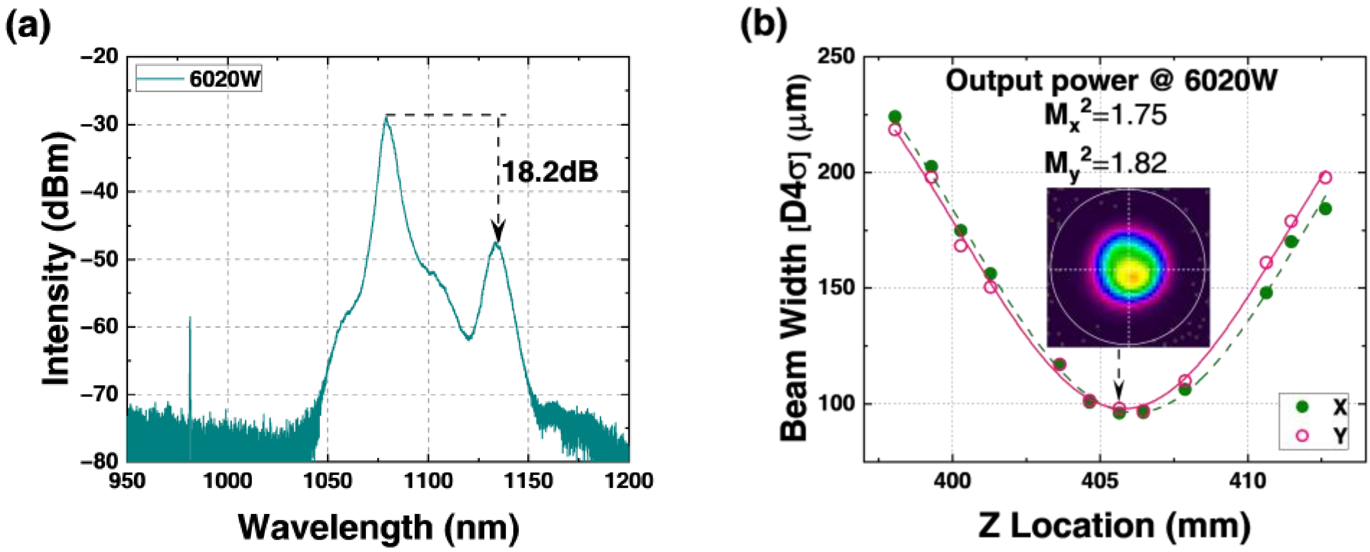

Figure 30. Experimental results of OAIFL based on SPF. (**a**) The spectrum when the output power is 6020 W (**b**) The beam quality at 6020 W [77].

The main experimental results from using SPF-CCCR and 25/400 µm CCAF are presented in Table 11 [106]. The comparison shows that in terms of power enhancement capability, the low-absorption design of the SPF-CCCR has a higher TMI threshold under unidirectional pump conditions, which can better support the high-power laser output by applying bidirectional pump. Despite the longer length of the SPF-CCCR, the larger equivalent core diameter gives it better SRS suppression. In this set of experiments, the SPF was perfectly used to balance SRS and TMI, achieving a 6 kW laser output with high beam quality.

Table 11. Comparison of the main results of applying SPF-CCCR and CCAF [77,106].

	Fiber Parameters		Power	SRS	TMI	M^2
	OS	AS				
Ref. [106]	22/400 µm 7.2 m	25/400 µm 13.5 m	5009 W	14.7 dB	>5009 W	2.83
This work	22/400 µm 4.32 m	SPF 21.0 m	6020 W	18.2 dB	>6060 W	1.77

5.3. Bidirectional-Output Fiber Laser Oscillator (2 × 3 kW) Based on SPF-CCCR

For the conventional structure of the fiber laser oscillator, due to the insufficient reflectivity of the HRFBG, it often produces part of the signal output from the other end of the HRFBG, and it is difficult to utilize this part of the power. In 2022, our group proposed a linear cavity, bidirectional-output fiber laser oscillator by replacing the HRFBG in the traditional fiber laser oscillator with the OCFBG [107]. This structure combines the bidirectional-output capability and the high-power output capability of conventional fiber lasers. In the previous work, wavelength-stabilized 976 nm LDs were used to pump CCAF with core/cladding diameter of 20/400 µm, and a bidirectional 2 kW laser output, which was limited by the pump power and SRS, was achieved. Using VCAF combined with other optimization measures is expected to improve the output power of bidirectional-output fiber lasers.

The laser structure of the bidirectional-output fiber laser oscillator based on the SPF-CCCR and the longitudinal structure of the fiber are shown in Figure 31. The pump source of the laser is non-wavelength-stabilized 976 nm LDs. In order to improve the pump ability of the laser, the pump light of 36 LDs with output power of about 250 W is coupled into the active fiber through two (18 + 1) ×1 backward pump/signal combiners. The SPF used is the same batch as the SPF used in Section 5.2. The diameter distribution of the fiber core/cladding and the pump absorption coefficient are consistent. The length distribution of each longitudinal section is 3 m–4 m–5 m–7 m–5 m, and the total length is 24 m. For better SRS suppression, the laser adopts a pair of OCFBGs with 3 dB bandwidth of 3 nm, and the reflectivity is ~10%.

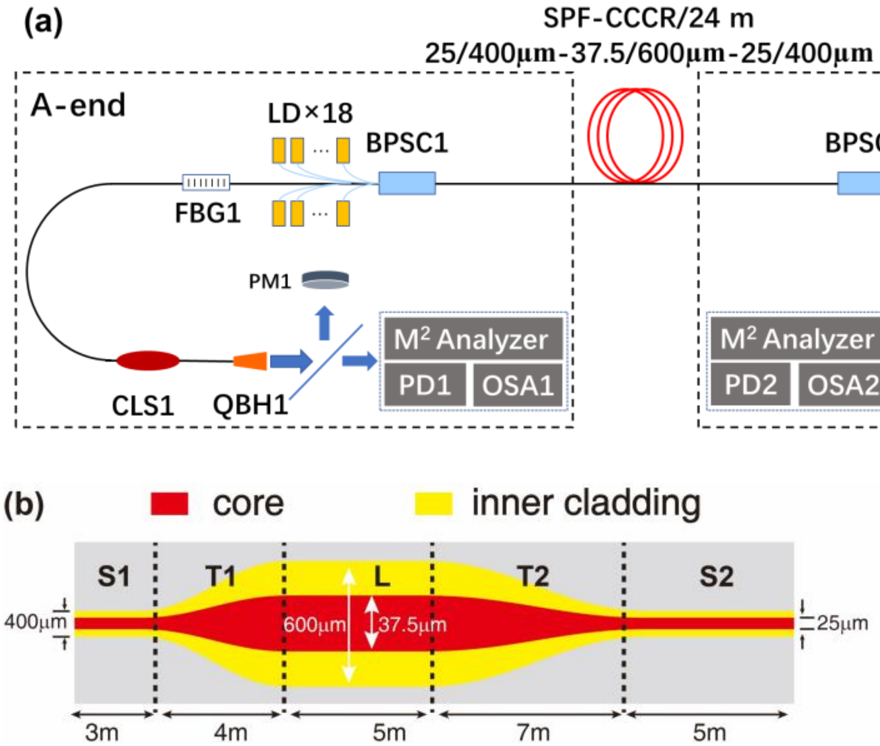

Figure 31. Schematic diagram of a bidirectional-output fiber laser oscillator based on SPF-CCCR. (**a**) Schematic diagram of laser structure. (**b**) Longitudinal structure diagram of the SPF-CCCR.

The final experimental results are shown in Figure 32. At the maximum output power, the output power at the two ends is 3256 W and 2840 W, respectively, with the total power and efficiency of 6096 W and 73.2%. No TMI appears, and the beam quality of the output laser at both ends is $M^2_{xA} = 2.06, M^2_{yA} = 1.90$ and $M^2_{xB} = 2.36, M^2_{yB} = 2.40$, respectively.

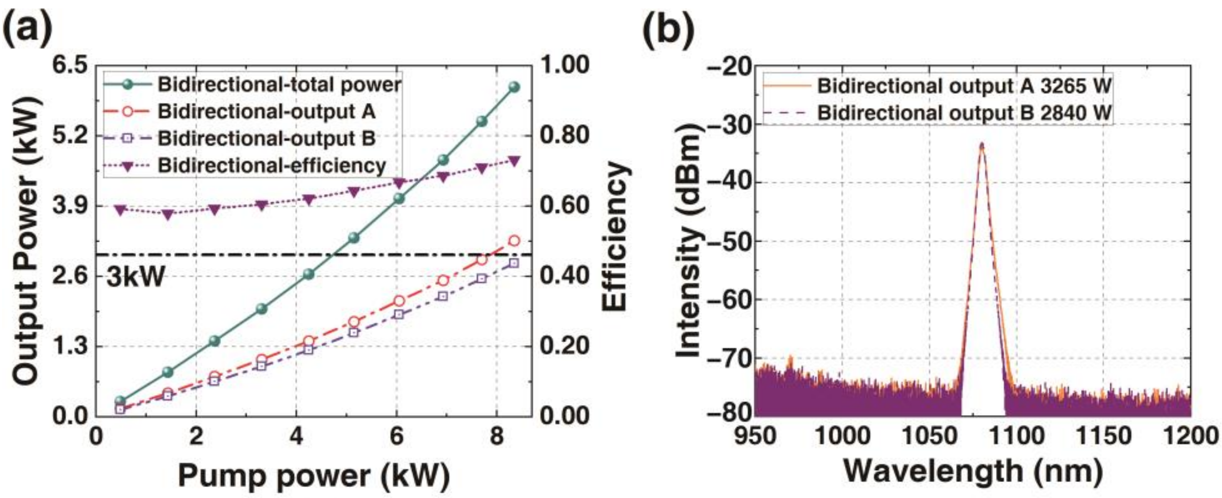

Figure 32. *Cont.*

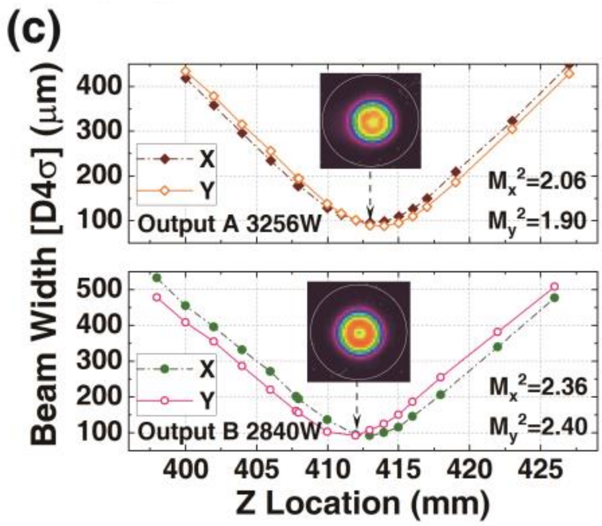

Figure 32. Results of the bidirectional-output oscillator in the bidirectional pump configuration. (**a**) Output power and efficiency at different pump powers. (**b**) Output spectra of A-end and B-end at the maximum output power. (**c**) Beam quality results of A-end and B-end at the maximum output power.

Figure 33 shows the comparison of the results of bidirectional-output fiber lasers based on SPF-CCCR and 25/400 μm CCAF. The 25/400 μm CCAF used for comparison has a total length of 28 m and a low absorption design (1.07 dB/ m@976 nm) to ensure a sufficiently high TMI threshold. Figure 33a,b show that under the unidirectional pump configuration, the total power when TMI occurs in the 25/400 μm CCAF-based laser is 2451 W (A-end pump) and 3156 W (B-end pump), respectively, which will limit the performance of the laser when applying the bidirectional pump configuration. Figure 33c shows the output spectra of both ends at their respective maximum output power when two kinds of fibers are applied. It can be found that when CCAF is applied, obvious SRS has appeared at lower output power. Therefore, whether from the perspective of TMI or SRS, the laser based on a uniform 25/400 μm fiber has limited power enhancement capability. Moreover, the results show that replacing the CCAF with SPF-CCCR can greatly increase the TMI threshold and effectively suppress SRS, thus ensuring the ability to achieve higher output power in the bidirectional pump configuration. However, the beam quality of the output laser becomes significantly worse, which may be caused by the offset of the fusion melting point or the larger coiling diameter of the SPF-CCCR.

5.4. Summary

From the results, the application of VCAF to QCW fiber lasers and OAIFL has achieved good results, and the output power and beam quality have been maintained well. Further optimization can further improve the output characteristics of the laser. It should be noted that due to the distinct natures of different lasers, QCW fiber lasers need to focus on the maintenance of beam quality and SRS suppression. OAIFL needs to pay more attention to the balance between SRS and TMI while controlling the beam quality. Compared with these two kinds of lasers, the current SPF-based bidirectional-output fiber laser oscillator has reached the power level of 2×3 kW, but the beam quality of the output laser is not ideal. The next step of optimization is to ensure the output power and improve the beam quality. Through the optimization of fiber design and fiber coiling, the output of near-single-mode laser with a bidirectional power of more than 3 kW can be predicted and realized.

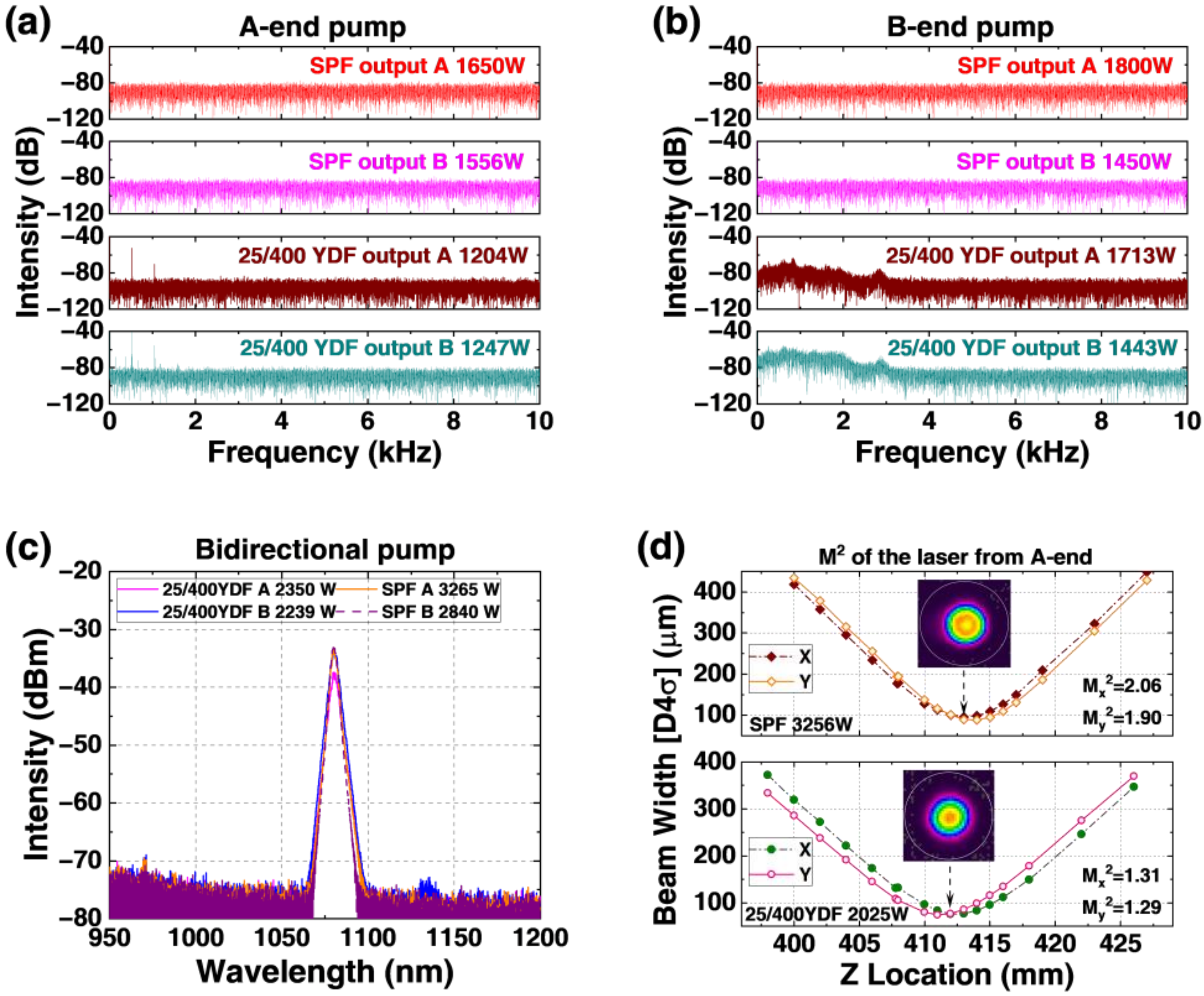

Figure 33. Comparison of output results of bidirectional-output fiber laser oscillator based on SPF-CCCR and 25/400 μm CCAF. (**a**) The frequency domain signal of the maximum output power under A-end pump configuration. (**b**) The frequency domain signal of the maximum output power under B-end pump configuration. (**c**) The spectra when the maximum output power is reached, respectively, under bidirectional pump. (**d**) Beam quality comparison of output laser at A-end.

6. Conclusions

Table 12 shows the maximum output power of various lasers based on different types of VCAF and the related results. At present, 6 kW continuous wave lasers are realized based on TF and SPF. In the experiment, the laser based on SPF and TF is compared with the laser based on CCAF under the same conditions. The results show that VCAF has greater advantages in improving the TMI threshold and suppressing SRS. In bidirectional-output fiber lasers, it is difficult to achieve high power (more than 3 kW in both directions) output based on CCAF, but higher power output can be easily achieved with SPF. In the above work, except that a few lasers are limited by the available pump power, TMI and SRS are still the limiting factors for further power scaling of VCAF-based fiber lasers and can be suppressed through further optimization of the fiber. In general, the enriched and developed VCAFs have shown great practical potential. Many comparative experiments show that the VCAF has a very good ability to balance nonlinear effect and TMI, which is an ideal scheme to achieve high-power fiber laser with excellent beam quality. In addition to the QCW and CW fiber lasers described above, the application of VCAF in pulsed fiber lasers is also worth anticipating.

Table 12. The maximum output power of different VCAFs in different laser types.

Fiber Type	Laser Type	Maximum Power/W	Threshold of TMI/W	M^2	SRS/dB
TF	CW Amplifier	6110	~5000	2.57	>45
SPF	CW Amplifier	6020	>6020	1.86	26.7
	OAIFL	6060	>6060	1.78	18.2
	Bidirectional-output Fiber Laser Oscillator	6096(3256 + 2840)	>6096	1.98/2.38	>40
SAF	CW Oscillator	1312	>1312	2.01	>40
	CW Amplifier	1816	1797	1.50	>40

At present, the main difficulty in the research of VCAF is the accurate fabrication of fiber. The fabrication method described in Section 2 can meet all the fabrication requirements of active fiber with a variable core diameter in various forms. In fact, the gradient form of VCAF is not limited to tapered, spindle, or saddle-shaped, and its cladding diameter variation mode is not limited to constant cladding diameter and a constant core-to-cladding ratio. However, the change of the core diameter in the length of several meters or even longer fiber is only in the order of micrometers. For the variable-speed drawing method, the accurate control of speed is particularly important. For the preform form control method, it is also a difficult point to make preforms according to the design values of the fiber. The inaccuracy of the VCAF fabrication may cause problems such as fiber mismatch, large transmission loss, and poor beam quality retention. As mentioned above, the structure parameters of the fiber also have an impact on the TMI and SRS of the laser. Current fabricating process cannot fabricate the fiber completely according to the design parameters, and it is almost impossible to ensure the consistency of the fiber parameters. The resulting performance differences are difficult to eliminate. However, we believe that the precise manufacturing technology of VCAF can be realized soon.

With the development of technology, VCAF will shine in various fields of fiber laser. In addition to the application in fiber laser with conventional structure and conventional wavelength, the operation wavelength of VCAF-based fiber lasers can be extended to the special wavelength, the laser polarization characteristics can be extended from the nonlinear polarization to the linear polarization, and so on. Moreover, not only in active fiber, but also vary core fiber can be used for laser delivery passive fiber in high-power laser. Due to the progress of technology and the traction of high-power laser demand, VCAF for single-frequency, polarization-maintaining, high peak power, especially CW high-power demand, has gradually moved from the laboratory to the market in recent years, greatly promoting the development of high-power fiber laser. Based on VCAF, combined with new pump source and other technology, it is expected to achieve industrial class near single-mode ($M^2 < 1.5$) fiber laser with output power greater than 10 kW and stable operation for a long time in the future.

Author Contributions: Conceptualization, X.W. and X.X. (Xiaojun Xu); methodology, X.W., C.S., B.Y., P.W. and X.X. (Xiaoming Xi); software, C.S., Y.Y. and L.Z.; validation, B.Y., Y.Y., L.Z., Z.P. and L.W.; formal analysis, K.H., H.Z. and X.X. (Xiaojun Xu); investigation, X.W., C.S. and H.Z.; resources, X.W., L.Z., Y.Y., L.W. and B.Y.; data curation, Y.Y. and L.Z.; writing—original draft preparation, L.Z. and X.W.; writing—review and editing, X.W. and X.X. (Xiaoming Xi); visualization, Y.Y. and L.W.; supervision, P.W., H.Z. and X.X. (Xiaoming Xi); project administration, X.X. (Xiaoming Xi), X.W. and H.Z.; funding acquisition, X.W. and X.X. (Xiaojun Xu). All authors have read and agreed to the published version of the manuscript.

Funding: This work is supported by Training Program for Excellent Young Innovations of Changsha (kq2206006).

Institutional Review Board Statement: Not applicable.

Informed Consent Statement: Not applicable.

Data Availability Statement: Not applicable.

Conflicts of Interest: The authors declare no conflict of interest.

References

1. Jauregui, C.; Limpert, J.; Tünnermann, A. High-power fibre lasers. *Nat. Photonics* **2013**, *7*, 861–867. [CrossRef]
2. Zuo, J.; Lin, X. High-Power Laser Systems. *Laser Photonics Rev.* **2022**, *16*, 2100741. [CrossRef]
3. Wang, Y.; Rintaro, K.; Kiyoyama, W.; Shirakura, Y.; Kurihara, T.; Nakanishi, Y.; Yamamoto, T.; Nakayama, M.; Ikoma, S.; Shima, K. 8-kW single-stage all-fiber Yb-doped fiber laser with a BPP of 0.50 mm-mrad. In Proceedings of the Fiber Lasers XVII: Technology and Systems, San Francisco, CA, USA, 1–6 February 2020.
4. Lin, H.; Xu, L.; Li, C.; Shu, Q.; Chu, Q.; Xie, L.; Guo, C.; Zhao, P.; Li, Z.; Wang, J.; et al. 10.6 kW high-brightness cascade-end-pumped monolithic fiber lasers directly pumped by laser diodes in step-index large mode area double cladding fiber. *Results Phys.* **2019**, *14*, 102479. [CrossRef]
5. Yang, B.; Wang, P.; Zhang, H.; Xi, X.; Shi, C.; Wang, X.; Xu, X. 6 kW single mode monolithic fiber laser enabled by effective mitigation of the transverse mode instability. *Opt. Express* **2021**, *29*, 26366. [CrossRef]
6. Ackermann, M.; Rehmann, G.; Lange, R.; Witte, U.; Safarzadeh, F.; Boden, B.; Weber, H.; Netz, D.; Perne, C.; Kösters, A.; et al. Extraction of more than 10 kW from a single ytterbium-doped MM-fiber. In Proceedings of the Fiber Lasers XVI: Technology and Systems, San Francisco, CA, USA, 2–7 February 2019.
7. Wen, Y.; Wang, P.; Xi, X.; Zhang, H.; Huang, L.; Yang, H.; Yan, Z.; Yang, B.; Shi, C.; Pan, Z.; et al. LD Direct Counter-Pumped 10 kW Fiber Laser Amplifier with Good Beam Quality. *Acta Phys. Sin.* **2022**, *71*, 2442202. [CrossRef]
8. Eidam, T.; Hanf, S.; Seise, E.; Andersen, T.V.; Gabler, T.; Wirth, C.; Schreiber, T.; Limpert, J.; Tunnermann, A. Femtosecond fiber CPA system emitting 830 W average output power. *Opt. Lett.* **2010**, *35*, 94–96. [CrossRef] [PubMed]
9. Smith, A.V.; Smith, J.J. Mode instability in high power fiber amplifiers. *Opt. Express* **2011**, *19*, 10180–10192. [CrossRef] [PubMed]
10. Zervas, M.N. Transverse mode instability, thermal lensing and power scaling in Yb^{3+}-doped high-power fiber amplifiers. *Opt. Express* **2019**, *27*, 19019–19041. [CrossRef] [PubMed]
11. Jauregui, C.; Stihler, C.; Limpert, J. Transverse mode instability. *Adv. Opt. Photonics* **2020**, *12*, 429–484. [CrossRef]
12. Rezaei-Nasirabad, R.; Azizi, S.; Paygan, D.; Tavassoli, M.; Abedinajafi, A.; Roohforouz, A.; Chenar, R.E.; Golshan, A.H.; Hejaz, K.; Vatani, V. 2.5 kW TMI-free co-pump Yb-doped fiber oscillator by 971.5 nm pumping wavelength. *Opt. Laser Technol.* **2023**, *157*, 108652. [CrossRef]
13. Wan, Y.; Yang, B.; Xi, X.; Zhang, H.; Wang, P.; Wang, X.; Xu, X. Comparison and Optimization on Transverse Mode Instability of Fiber Laser Amplifier Pumped by Wavelength-Stabilized and Non-Wavelength-Stabilized 976 nm Laser Diode. *IEEE Photonics J.* **2022**, *14*, 1–5. [CrossRef]
14. Wan, Y.; Xi, X.; Yang, B.; Zhang, H.; Wang, X. Enhancement of TMI Threshold in Yb-Doped Fiber Laser by Optimizing Pump Wavelength. *IEEE Photonics Technol. Lett.* **2021**, *33*, 656–659. [CrossRef]
15. Tao, R.; Ma, P.; Wang, X.; Zhou, P.; Liu, Z. Mitigating of modal instabilities in linearly-polarized fiber amplifiers by shifting pump wavelength. *J. Opt.* **2015**, *17*, 45504. [CrossRef]
16. Roohforouz, A.; Chenar, R.E.; Azizi, S.; Abad, R.R.N.; Hejaz, K.; Najafi, A.A.; Vatani, V.; Nabavi, S.H. Effect of pumping configuration on the transverse mode instability power threshold in a 3.02 kW fiber laser oscillator. In Proceedings of the Advanced Solid State Lasers, Vienna, Austria, 29 September–3 October 2019.
17. Shi, C.; Su, R.T.; Zhang, H.W.; Yang, B.L.; Wang, X.L.; Zhou, P.; Xu, X.J.; Lu, Q.S. Experimental Study of Output Characteristics of Bi-Directional Pumping High Power Fiber Amplifier in Different Pumping Schemes. *IEEE Photonics J.* **2017**, *9*, 1–10. [CrossRef]
18. Jauregui, C.; Otto, H.; Breitkopf, S.; Limpert, J.; Tünnermann, A. Optimizing high-power Yb-doped fiber amplifier systems in the presence of transverse mode instabilities. *Opt. Express* **2016**, *24*, 7879–7892. [CrossRef]
19. Sanjabi Eznaveh, Z.; López-Galmiche, G.; Antonio-López, E.; Amezcua Correa, R.; Shaw, L.B. Bi-directional pump configuration for increasing thermal modal instabilities threshold in high power fiber amplifiers. In Proceedings of the Fiber Lasers XII: Technology, Systems, and Applications, San Francisco, CA, USA, 7–12 February 2015.
20. Luo, X.; Tao, R.; Shi, C.; Zhang, H.; Wang, X.; Zhou, P.; Xu, X. Power of all-fiber amplifier increasing from 1030 W to 2280 W through suppressing mode instability by increasing the seed power. *Chin. Phys. B* **2019**, *28*, 24208. [CrossRef]
21. Tao, R.; Wang, X.; Zhou, P.; Liu, Z. Seed power dependence of mode instabilities in high-power fiber amplifiers. *J. Opt* **2017**, *19*, 65202. [CrossRef]
22. Ma, X.; Zhu, C.; Hu, I.; Kaplan, A.; Galvanauskas, A. Single-mode chirally-coupled-core fibers with larger than 50µm diameter cores. *Opt. Express* **2014**, *22*, 9206–9219. [CrossRef]
23. Stutzki, F.; Jansen, F.; Eidam, T.; Steinmetz, A.; Jauregui, C.; Limpert, J.; Tunnermann, A. High average power large-pitch fiber amplifier with robust single-mode operation. *Opt. Lett.* **2011**, *36*, 689–691. [CrossRef]

24. Hejaz, K.; Norouzey, A.; Poozesh, R.; Heidariazar, A.; Roohforouz, A.; Rezaei Nasirabad, R.; Tabatabaei Jafari, N.; Hamedani Golshan, A.; Babazadeh, A.; Lafouti, M. Controlling mode instability in a 500 W ytterbium-doped fiber laser. *Laser Phys.* **2014**, *24*, 25102. [CrossRef]
25. Huang, Z.; Shu, Q.; Luo, Y.; Tao, R.; Feng, X.; Liu, Y.; Lin, H.; Wang, J.; Jing, F. 3.5 kW narrow-linewidth monolithic fiber amplifier at 1064 nm by employing a confined doping fiber. *J. Opt. Soc. Am. B* **2021**, *38*, 2945–2952. [CrossRef]
26. Zhang, F.; Wang, Y.; Lin, X.; Cheng, Y.; Zhang, Z.; Liu, Y.; Liao, L.; Xing, Y.; Yang, L.; Dai, N.; et al. Gain-tailored Yb/Ce codoped aluminosilicate fiber for laser stability improvement at high output power. *Opt. Express* **2019**, *27*, 20824–20836. [CrossRef] [PubMed]
27. Liao, L.; Zhang, F.; He, X.; Chen, Y.; Wang, Y.; Li, H.; Peng, J.; Yang, L.; Dai, N.; Li, J. Confined-doped fiber for effective mode control fabricated by MCVD process. *Appl. Opt. Opt. Technol. Biomed. Opt.* **2018**, *57*, 3244–3249. [CrossRef] [PubMed]
28. Yuan, M.; Sui, Y.; Bai, Z.; Fan, Z. Recent Advances in Chirally-Coupled Core Fibers. *Front. Phys.* **2022**, *10*, 950492. [CrossRef]
29. Hochheim, S.; Brockmuller, E.; Wessels, P.; Koponen, J.; Lowder, T.; Novotny, S.; Willke, B.; Neumann, J.; Kracht, D. Single-Frequency 336 W Spliceless All-Fiber Amplifier Based on a Chirally-Coupled-Core Fiber for the Next Generation of Gravitational Wave Detectors. *J. Light. Technol.* **2022**, *40*, 2136–2143. [CrossRef]
30. Zhan, H.; Liu, Q.; Wang, Y.; Ke, W.; Ni, L.; Wang, X.; Peng, K.; Gao, C.; Li, Y.; Lin, H.; et al. 5kW GTWave fiber amplifier directly pumped by commercial 976nm laser diodes. *Opt. Express* **2016**, *24*, 27087–27095. [CrossRef]
31. Filippov, V.; Chamorovskii, Y.; Kerttula, J.; Golant, K.; Pessa, M.; Okhotnikov, O.G. Double clad tapered fiber for high power applications. *Opt. Express* **2008**, *16*, 1929–1944. [CrossRef]
32. Trikshev, A.I.; Kurkov, A.S.; Tsvetkov, V.B.; Filatova, S.A.; Kertulla, J.; Filippov, V.; Chamorovskiy, Y.K.; Okhotnikov, O.G. A 160 W single-frequency laser based on an active tapered double-clad fiber amplifier. *Laser Phys. Lett.* **2013**, *10*, 65101. [CrossRef]
33. Zhou, Z.; Zhang, H.; Wang, X.; Pan, Z.; Su, R.; Yang, B.; Zhou, P.; Xu, X. All-fiber-integrated single frequency tapered fiber amplifier with near diffraction limited output. *J. Opt.* **2016**, *18*, 65504. [CrossRef]
34. Pierre, C.; Guiraud, G.; Vincont, C.; Traynor, N.; Santarelli, G.; Boullet, J. 120W single frequency laser based on short active double clad tapered fiber. In Proceedings of the European Conference on Lasers and Electro-Optics 2017, Munich, Germany, 25–29 June 2017.
35. Noronen, T.; Fedotov, A.; Rissanen, J.; Gumenyuk, R.; Butov, O.; Chamorovskii, Y.; Golant, K.; Odnoblyudov, M.; Filippov, V.; Hartl, I.; et al. Ultra-large mode area single frequency anisotropic MOPA with double clad Yb-doped tapered fiber. In Proceedings of the Fiber Lasers XV: Technology and Systems, San Francisco, CA, USA, 27 January–1 February 2018.
36. Huang, L.; Zhou, Z.; Shi, C.; Tao, R.; Ma, P.; Wang, X.; Zhou, P. Towards tapered-fiber-based all-fiberized high power narrow linewidth fiber laser. *Sci. China. Technol. Sci.* **2018**, *61*, 971–981. [CrossRef]
37. Lai, W.; Ma, P.; Liu, W.; Huang, L.; Li, C.; Ma, Y.; Zhou, P. 550 W single frequency fiber amplifiers emitting at 1030 nm based on a tapered Yb-doped fiber. *Opt. Express* **2020**, *28*, 20908–20919. [CrossRef] [PubMed]
38. Huang, L.; Lai, W.; Ma, P.; Wang, J.; Su, R.; Ma, Y.; Li, C.; Zhi, D.; Zhou, P. Tapered Yb-doped fiber enabled monolithic high-power linearly polarized single-frequency laser. *Opt. Lett.* **2020**, *45*, 4001–4004. [CrossRef] [PubMed]
39. Kerttula, J.; Filippov, V.; Chamorovskii, Y.; Golant, K.; Okhotnikov, O.G. Actively Q-switched 1.6-mJ tapered double-clad ytterbium-doped fiber laser. *Opt. Express* **2010**, *18*, 18543–18549. [CrossRef] [PubMed]
40. Gumenyuk, R.; Filippov, V.; Vorotinskii, A.; Okhotnikov, O.G.; Chamorovskii, Y.; Golant, K. All-fiber, high-power, picosecond Yb double clad tapered fiber amplifier. In Proceedings of the 2014 International Conference Laser Optics, St. Petersburg, Russia, 30 June–4 July 2014.
41. Koptev, M.Y.; Anashkina, E.A.; Bobkov, K.K.; Likhachev, M.E.; Levchenko, A.E.; Aleshkina, S.S.; Semjonov, S.L.; Denisov, A.N.; Bubnov, M.M.; Lipatov, D.S.; et al. Fibre amplifier based on an ytterbium-doped active tapered fibre for the generation of megawatt peak power ultrashort optical pulses. *Quantum Electron.* **2015**, *45*, 443–450. [CrossRef]
42. Mu, X.; Steinvurzel, P.; Belden, P.; Rose, T.; Lotshaw, W.; Beck, S. Nanosecond-Pulsed, mJ-Level Single-Mode Fiber Master Oscillator Power Amplifier with Polarization Maintaining Tapered Gain Fiber. In Proceedings of the Lasers Congress 2016 (ASSL, LSC, LAC), Boston, MA, USA, 30 October–3 November 2016; OSA: Washington, DC, USA, 2016.
43. Roy, V.; Paré, C.; Labranche, B.; Laperle, P.; Desbiens, L.; Boivin, M.; Taillon, Y.; Robin, C.A.; Hartl, I. Yb-doped large mode area tapered fiber with depressed cladding and dopant confinement. In Proceedings of the Fiber Lasers XIV: Technology and Systems, San Francisco, CA, USA, 28 January–2 February 2017.
44. Zhu, Y.; Lorenz, M.; Leich, M.; Grimm, S.; Aichele, C.; Kobelke, J.; Bartelt, H.; Jager, M. Laser peak power scaling and beam quality improvement with a tapered ytterbium rod-type amplifier made by powder sinter technology. In Proceedings of the The European Conference on Lasers and Electro-Optics 2017, Munich, Germany, 25–29 June 2017.
45. Zhu, Y.; Eschrich, T.; Leich, M.; Grimm, S.; Kobelke, J.; Lorenz, M.; Bartelt, H.; Jäger, M. Yb^{3+}-doped rod-type amplifiers with local adiabatic tapers for peak power scaling and beam quality improvement. *Laser Phys.* **2017**, *27*, 105103. [CrossRef]
46. Filippov, V.; Vorotynskii, A.; Noronen, T.; Gumenyuk, R.; Chamorovskii, Y.; Golant, K.; Robin, C.A.; Hartl, I. Picosecond MOPA with ytterbium doped tapered double clad fiber. In Proceedings of the Fiber Lasers XIV: Technology and Systems, San Francisco, CA, USA, 28 January–2 February 2017.
47. Bobkov, K.; Andrianov, A.; Koptev, M.; Muravyev, S.; Levchenko, A.; Velmiskin, V.; Aleshkina, S.; Semjonov, S.; Lipatov, D.; Guryanov, A.; et al. Sub-MW peak power diffraction-limited chirped-pulse monolithic Yb-doped tapered fiber amplifier. *Opt. Express* **2017**, *25*, 26958–26972. [CrossRef]

48. Noronen, T.; Gumenyuk, R.; Chamorovskii, Y.; Golant, K.; Odnoblyudov, M.; Filippov, V. Ultrafast picosecond MOPA With Yb-doped tapered double clad fiber. In Proceedings of the 2017 Conference on Lasers and Electro Optics Europe & European Quantum lectronics Conference (CLEO/Europe-EQEC), Munich, Germany, 25–29 June 2017.
49. Bobkov, K.; Levchenko, A.; Aleshkina, S.; Semenov, S.; Denisov, A.; Bubnov, M.; Lipatov, D.; Laptev, A.; Guryanov, A.; Likhachev, M. 1.5 MW peak power diffraction limited monolithic Yb-doped tapered fiber amplifier. In Proceedings of the 2017 Conference on Lasers and Electro-Optics Europe & European Quantum Electronics Conference (CLEO/Europe-EQEC), Munich, Germany, 25–29 June 2017.
50. Noronen, T.; Gumenyuk, R.; Chamorovskii, Y.; Golant, K.; Odnoblyudov, M.; Filippov, V. Anisotropic Ultra-Large Mode Area Yb-doped Tapered Double Clad Fiber For Ultrafast Amplifiers. In Proceedings of the Laser Congress 2017 (ASSL, LAC), Nagoya, Aichi, Japan, 1–5 October 2017.
51. Fedotov, A.; Noronen, T.; Gumenyuk, R.; Ustimchik, V.; Chamorovskii, Y.; Golant, K.; Odnoblyudov, M.; Rissanen, J.; Niemi, T.; Filippov, V. Ultra-large core birefringent Yb-doped tapered double clad fiber for high power amplifiers. *Opt. Express* **2018**, *26*, 6581–6592. [CrossRef]
52. Khudyakov, M.M.; Levchenko, A.E.; Velmiskin, V.V.; Bobkov, K.K.; Lipatov, D.S.; Guryanov, A.N.; Bubnov, M.M.; Likhachev, M.E.; Likhachev, B.A.M.E. 107-kW-Peak-Power 2-ns Pulse Tapered Er-doped Fiber Amplifier. In Proceedings of the 2018 International Conference Laser Optics (ICLO), St. Petersburg, Russia, 4–8 June 2018.
53. Huang, L.; Lai, W.; Su, R.; Ma, P.; Jiang, M.; Wu, J.; Ma, Y.; Zhou, P. Monolithic Linearly Polarized Nanosecond Fiber Laser with Record Peak Power and Near-Transform-Limited Linewidth. In Proceedings of the 18th International Conference on Optical Communications and Networks, Huangshan, China, 5–8 August 2019.
54. Bobkov, K.K.; Levchenko, A.E.; Velmiskin, V.V.; Kochergina, T.A.; Aleshkina, S.S.; Bubnov, M.M.; Lipatov, D.S.; Guryanov, A.N.; Likhachev, M.E. High Peak and Average Power Yb-Doped Tapered Fiber Amplifier. In Proceedings of the CLEO: Sci-ence and Innovations 2019, San Jose, CA, USA, 5–10 May 2019.
55. Rissanen, J.; Fedotov, A.; Noronen, T.; Gumenyuk, R.; Chamorovskiy, Y.; Kolosovskii, A.; Voloshin, V.; Vorobev, I.; Odnoblyudov, M.; Filippov, V.; et al. Large-mode-area double clad ytterbium-doped tapered fiber with circular birefringence. In Proceedings of the Fiber Lasers XVI: Technology and Systems, San Francisco, CA, USA, 4–7 February 2019.
56. Andrianov, A.V.; Koptev, M.Y.; Anashkina, E.A.; Muravyev, S.V.; Kim, A.V.; Lipatov, D.S.; Velmiskin, V.V.; Levchenko, A.E.; Bubnov, M.M.; Likhachev, M.E. Tapered erbium-doped fibre laser system delivering 10 MW of peak power. *Quantum Electron.* **2019**, *49*, 1093–1099. [CrossRef]
57. Bobkov, K.K.; Likhachev, M.E.; Levchenko, A.E.; Velmiskin, V.V.; Kochergina, T.A.; Aleshkina, S.S.; Bubnov, M.M.; Lipatov, D.S.; Laptev, A.Y.; Guryanov, A.N. 71 W Average Power Sub-MW Peak Power Diffraction-Limited Monolithic Tapered Fiber Amplifier. In Proceedings of the 2019 Conference on Lasers and Electro-Optics Europe & European Quantum Electronics Conference (CLEO/Europe-EQEC), Munich, Germany, 23–27 June 2019.
58. Leich, M.; Kalide, A.; Eschrich, T.; Lorenz, M.; Lorenz, A.; Wondraczek, K.; Schönfeld, D.; Langner, A.; Schötz, G.; Jäger, M. 2 MW peak power generation in fluorine co-doped Yb fiber prepared by powder-sinter technology. *Opt. Lett.* **2020**, *45*, 4404–4407. [CrossRef]
59. Petrov, A.; Odnoblyudov, M.; Gumenyuk, R.; Minyonok, L.; Chumachenko, A.; Filippov, V. Picosecond Yb-doped tapered fiber laser system with 1.26 MW peak power and 200 W average output power. *Sci. Rep.* **2020**, *10*, 17781. [CrossRef]
60. Guesmi, K.; Mugnier, A.; Canat, G.; Canal, C.; Maine, P.; Zervas, M.N.; Jauregui-Misas, C. Simple design for high energy femtosecond tapered double clad fiber amplifier. In Proceedings of the Fiber Lasers XVIII: Technology and Systems, Online Only, 6–11 March 2021.
61. Scol, F.; Bouwmans, G.; Hugonnot, E. High-energy, narrow-linewidth, flat-top temporal profile nanosecond-pulses from ytterbium-doped tapered fiber amplifier with chirped-diode seeding. *OSA Contin.* **2021**, *4*, 1162–1169. [CrossRef]
62. Petrov, A.; Mikhailovsky, G.; Gorbatchev, A.; Odnoblyudov, M.; Kozlyakov, M.; Rissanen, J.; Gumenyuk, R.; Filippov, V.; Zervas, M.N.; Jauregui-Misas, C. High-power and pulse energy picosecond narrow linewidth laser system based on tapered fiber amplifier for second harmonic generation. In Proceedings of the Fiber Lasers XVIII: Technology and Systems, Online Only, 6–11 March 2021.
63. Zhu, Y.; Leich, M.; Lorenz, M.; Eschrich, T.; Aichele, C.; Kobelke, J.; Bartelt, H.; Jäger, M. Yb-doped large mode area fiber for beam quality improvement using local adiabatic tapers with reduced dopant diffusion. *Opt. Express* **2018**, *26*, 17034–17043. [CrossRef] [PubMed]
64. Filippov, V.; Chamorovskii, Y.; Kerttula, J.; Kholodkov, A.; Okhotnikov, O.G. Single-mode 212 W tapered fiber laser pumped by a low-brightness source. *Opt. Lett.* **2008**, *33*, 1416–1418. [CrossRef]
65. Filippov, V.; Chamorovskii, Y.; Kerttula, J.; Kholodkov, A.; Okhotnikov, O.G. 600 W power scalable single transverse mode tapered double-clad fiber laser. *Opt. Express* **2009**, *17*, 1203–1214. [CrossRef] [PubMed]
66. Filippova, V.; Chamorovskiib, Y.; Kerttula, J.; Kholodkov, A.; Okhotnikova, O.G. High-power single-mode tapered double-clad ytterbium fiber laser pumped by diode-laser bar. In Proceedings of the Fiber Lasers VI: Technology, Systems, and Applications, San Jose, CA, USA, 24–29 January 2009.
67. Filippov, V.; Kerttula, J.; Chamorovskii, Y.; Golant, K.; Okhotnikov, O.G. Highly efficient 750 W tapered double-clad ytterbium fiber laser. *Opt. Express* **2010**, *18*, 12499–12512. [CrossRef]

68. Lin, X.; Zhang, Z.; Chu, Y.; Wang, Y.; Xing, Y.; Chen, G.; Peng, J.; Li, H.; Dai, N.; Li, J. Fabrication and laser performance of cladding uniform core tapered fiber. *Opt. Fiber Technol.* **2021**, *64*, 102561. [CrossRef]
69. Lin, X.; Ye, Y.; Zhang, Z.; Wang, X.; Xing, Y.; Chen, G.; Peng, J.; Li, H.; Dai, N.; Li, J. 2.7 kW co-pumped fiber amplifier based on constant-cladding tapered-core fiber. *Opt. Fiber Technol.* **2022**, *68*, 102773. [CrossRef]
70. Zeng, L.; Xi, X.; Ye, Y.; Zhang, H.; Wang, X.; Pan, Z.; Wang, Z.; Xu, X. Near-single-mode 3 kW monolithic fiber oscillator based on a longitudinally spindle-shaped Yb-doped fiber. *Opt. Lett.* **2020**, *45*, 5792–5795. [CrossRef]
71. Zeng, L.; Xi, X.; Ye, Y.; Lin, X.; Wang, X.; Li, J.; Shi, C.; Yang, B.; Zhang, H.; Wang, P.; et al. A novel fiber laser oscillator employing saddle-shaped core ytterbium-doped fiber. *Appl. Phys. B* **2020**, *126*, 185. [CrossRef]
72. Ye, Y.; Lin, X.; Xi, X.; Shi, C.; Yang, B.; Zhang, H.; Wang, X.; Li, J.; Xu, X. Novel constant-cladding tapered-core ytterbium-doped fiber for high-power fiber laser oscillator. *High Power Laser Sci.* **2021**, *9*, 142–148. [CrossRef]
73. Ye, Y.; Lin, X.; Xi, X.; Zhang, H.; Yang, B.; Shi, C.; Wang, X.; Li, J.; Xu, X. Demonstration of constant-cladding tapered-core Yb-doped fiber for mitigating thermally-induced mode instability in high-power monolithic fiber amplifiers. *Opt. Express* **2022**, *30*, 24936–24947. [CrossRef] [PubMed]
74. An, Y.; Yang, H.; Xiao, H.; Chen, X.; Huang, L.; Pan, Z.; Wang, X.; Xi, X.; Ma, P.; Wang, Z. 4-kW single-mode laser output using homemade double-tapered fiber. *Chin. J. Lasers* **2020**, *1*, 115002.
75. Song, J.; Ren, S.; Wang, G.; Yang, H.; Chen, Y.; Ma, P.; Liu, W.; Huang, L.; Pan, Z.; Zhou, P. High power narrow-linewidth fiber laser based on double-tapered fiber. *J. Light. Technol.* **2022**, *40*, 5668–5672. [CrossRef]
76. Zhang, Z.; Lin, X.; Zhang, X.; Luo, Y.; Liao, S.; Wang, X.; Chen, G.; Xing, Y.; Li, H.; Peng, J.; et al. Low-numerical aperture confined-doped long-tapered Yb-doped silica fiber for a single-mode high-power fiber amplifier. *Opt. Express* **2022**, *30*, 32333–32346. [CrossRef]
77. Zeng, L.; Yang, H.; Xi, X.; Ye, Y.; Huang, L.; Yang, B.; Zhang, H.; Yan, Z.; Wang, X.; Pan, Z.; et al. Optimization and demonstration of 6 kW oscillating-amplifying integrated fiber laser employing spindle-shaped fiber to suppress SRS and TMI. *Opt. Laser Technol.* **2023**, *159*, 108903. [CrossRef]
78. Kerttula, J.; Filippov, V.; Chamorovskii, Y.; Ustimchik, V.; Golant, K.; Okhotnikov, O.G. Tapered fiber amplifier with high gain and output power. *Laser Phys.* **2012**, *22*, 1734–1738. [CrossRef]
79. Filippov, V.; Chamorovskii, Y.K.; Golant, K.M.; Vorotynskii, A.; Okhotnikov, O.G.; Ballato, J. Optical Amplifiers and Lasers Based on Tapered Fiber Geometry for Power and Energy Scaling with Low Signal Distortion. In Proceedings of the Fiber Lasers XIII: Technology, Systems, and Applications, San Francisco, CA, USA, 13–18 February 2016.
80. Shi, C.; Zhang, H.; Wang, X.; Zhou, P.; Xu, X. kW-class high power fiber laser enabled by active long tapered fiber. *High Power Laser Sci.* **2018**, *6*, 1–5. [CrossRef]
81. Zhang, H.; Yang, B.; Wang, X.; Shi, C.; Zhou, P.; Xu, X. High Power All-Fiberized Oscillator Based on Tapered Fiber. In Proceedings of the Conference on Lasers and Electro-Optics/Pacific Rim 2018, Hong Kong, China, 29 July–3 August 2018.
82. Patokoski, K.; Rissanen, J.; Noronen, T.; Gumenyuk, R.; Chamorovskii, Y.; Filippov, V.; Toivonen, J. Single-frequency 100 ns/05 mJ laser pulses from all-fiber double clad ytterbium doped tapered fiber amplifier. *Opt. Express* **2019**, *27*, 31532–31541. [CrossRef]
83. Huang, L.; Ma, P.; Su, R.; Lai, W.; Ma, Y.; Zhou, P. Comprehensive investigation on the power scaling of a tapered Yb-doped fiber-based monolithic linearly polarized high-peak-power near-transform-limited nanosecond fiber laser. *Opt. Express* **2021**, *29*, 761–782. [CrossRef]
84. Yang, B.; Zhang, H.; Shi, C.; Wang, X.; Pan, Z.; Wang, Z.; Zhou, P.; Xu, X. High power monolithic tapered ytterbium-doped fiber laser oscillator. *Opt. Express* **2019**, *27*, 7585–7592. [CrossRef]
85. Ye, Y.; Xi, X.; Shi, C.; Yang, B.; Wang, X.; Zhang, H.; Zhou, P.; Xu, X. Comparative study on transverse mode instability of fiber amplifiers based on long tapered fiber and conventional uniform fiber. *Laser Phys. Lett.* **2019**, *16*, 85109. [CrossRef]
86. Fedotov, A.; Ustimchik, V.; Chamorovskii, Y.; Gumenyuk, R.; Filippov, V. Low-birefringence Active Tapered Fibers for High-power Applications. In Proceedings of the Specialty Optical Fibers 2020, Washington, DC, USA, 13–16 July 2020.
87. Zeng, L.; Xi, X.; Ye, Y.; Wang, X.; Yang, B.; Pan, Z.; Shi, C.; Zhang, H.; Wang, P.; Wang, Z.; et al. A 1.8 kW fiber laser oscillator employing a section of spindle-shaped core ytterbium-doped fiber. *Laser Phys. Lett.* **2020**, *17*, 95104. [CrossRef]
88. Ye, Y.; Lin, X.; Xi, X.; Zeng, L.; Yang, B.; Zhang, H.; Wang, X.; Li, J.; Xu, X. 2 kW monolithic fiber amplifier based on constant-cladding tapered-core Yb-doped fiber. In Proceedings of the 24th National Laser Conference & Fifteenth National Conference on Laser Technology and Optoelectronics, Shanghai, China, 17–20 October 2020.
89. Fedotov, A.; Ustimchik, V.; Rissanen, J.; Kolosovskii, A.; Voloshin, V.; Vorob Ev, I.; Gumenyuk, R.; Chamorovskiy, Y.; Filippov, V. Active tapered double-clad fiber with low birefringence. *Opt. Express* **2021**, *29*, 16506–16519. [CrossRef] [PubMed]
90. Fedotov, A.; Ustimchik, V.; Rissanen, J.; Noronen, T.; Gumenyuk, R.; Chamorovskii, Y.; Kolosovskii, A.; Voloshin, V.; Vorob'Ev, I.; Filippov, V.; et al. Large mode area double-clad ytterbium-doped tapered fiber with low birefringence. In Proceedings of the Fiber Lasers XVIII: Technology and Systems, Online Only, 6–12 March 2021.
91. Bobkov, K.K.; Aleshkina, S.S.; Khudyakov, M.M.; Lipatov, D.S.; Likhachev, M.E.; Kalli, K.; Mendez, A.; Peterka, P. Active tapered fibers for high peak power fiber lasers. In Proceedings of the SPIE Optics + Optoelectronics, Online Only, 19–30 April 2021.
92. Zeng, L.; Pan, Z.; Xi, X.; Yang, H.; Ye, Y.; Huang, L.; Zhang, H.; Wang, X.; Wang, Z.; Zhou, P.; et al. 5 kW monolithic fiber amplifier employing homemade spindle-shaped ytterbium-doped fiber. *Opt. Lett.* **2021**, *46*, 1393–1396. [CrossRef] [PubMed]

93. Li, W.; Ma, P.; Lai, W.; Song, J.; Wang, T.; Ren, B.; Liu, W.; Zhou, P.; Si, L. Tapered active fiber simultaneously enabled 141 W high average and 1.3 MW high peak power via all-fiber and polarization-maintained picosecond amplifier. *Opt. Laser Technol.* **2022**, *152*, 108166. [CrossRef]
94. Li, W.; Ma, P.; Chen, Y.; Song, J.; Lai, W.; Liu, W.; Zhou, P.; Si, L. 694 W sub-GHz polarization-maintained tapered fiber amplifier based on spectral and pump wavelength optimization. *Opt. Express* **2022**, *30*, 26875–26885. [CrossRef]
95. Ye, Y.; Lin, X.; Yang, B.; Xi, X.; Shi, C.; Zhang, H.; Wang, X.; Li, J.; Xu, X. Tapered Yb-doped fiber enabled a 4 kW near-single-mode monolithic fiber amplifier. *Opt. Lett.* **2022**, *47*, 2162–2165. [CrossRef]
96. Wang, L.; Zhang, H.; Wang, P.; Yang, B.; Wang, X.; Ning, Y.; Xu, X. A 6.4-kW peak power near-single-mode quasi-continuous wave fiber laser oscillator employing spindle-shaped ytterbium-doped fiber. *Opt. Laser Technol.* **2022**, *154*, 108338. [CrossRef]
97. Wang, L.; Zhang, H.; Wang, P.; Yang, B.; Wang, X.; Ning, Y.; Xu, X. Theoretical and Experimental Study of High-Peak-Power High-Brightness Quasi-CW Fiber Laser. *IEEE Photonics J.* **2022**, *14*, 1–6.
98. Shiraki, K.; Ohashi, M.; Tateda, M. Suppression of stimulated Brillouin scattering in a fibre by changing the core radius. *Electron. Lett.* **1995**, *31*, 668–669. [CrossRef]
99. Filippov, V.; Kerttula, J.; Chamorovskii, Y.; Golant, K.; Okhotnikova, O.G. Actively Q-switched ytterbium tapered fiber laser. In Proceedings of the Fiber Lasers VIII: Technology, Systems, and Applications, San Francisco, CA, USA, 22–27 January 2011.
100. Zeng, L.; Shi, C.; Xi, X.; Zhang, H.; Wang, X.; Xu, X.; Zhao, Y. Study on stimulated Raman scattering in fiber amplifier employing tapered Yb^{3+} doped fiber. In Proceedings of the Fifth International Symposium on Laser Interaction with Matter, Changsha, China, 11–14 November 2018.
101. SeeFiberLaser. Available online: http://www.seelight.net/html/SFLaser/index.html (accessed on 1 December 2022).
102. Shi, C.; Wang, X.; Zhou, P.; Xu, X.; Lu, Q. Theoretical study of mode evolution in active long tapered multimode fiber. *Opt. Express* **2016**, *24*, 19473–19490. [CrossRef] [PubMed]
103. Ye, Y.; Lin, X.; Xi, X.; Zhang, H.; Wang, X.; Li, J.; Xu, X. Large mode area saddle-shaped core Yb-doped fiber enabled monolithic high-power, high-efficiency, near-diffraction-limited MOPA laser. In Proceedings of the Thirteenth International Conference on Information Optics and Photonics (CIOP 2022), Xi'an, China, 7–10 August 2022.
104. Yang, B.; Zhang, H.; Shi, C.; Tao, R.; Su, R.; Ma, P.; Wang, X.; Zhou, P.; Xu, X.; Lu, Q. 3.05 kW monolithic fiber laser oscillator with simultaneous optimizations of stimulated Raman scattering and transverse mode instability. *J. Opt.* **2018**, *20*, 25802. [CrossRef]
105. Hong, Z.; Wan, Y.; Xi, X.; Zhang, H.; Wang, X.; Xu, X. High-peak-power pump-modulated quasi-CW fiber laser. *Appl. Opt.* **2022**, *61*, 1826–1833. [CrossRef] [PubMed]
106. Zeng, L.; Xi, X.; Zhang, H.; Yang, B.; Wang, P.; Wang, X.; Xu, X. Demonstration of the reliability of a 5-kW-level oscillating–amplifying integrated fiber laser. *Opt. Lett.* **2021**, *46*, 5778–5781. [CrossRef] [PubMed]
107. Zhong, P.; Wang, L.; Yang, B.; Zhang, H.; Xi, X.; Wang, P.; Wang, X. 2×2 kW near-single-mode bidirectional high-power output from a single-cavity monolithic fiber laser. *Opt. Lett.* **2022**, *47*, 2806–2809. [CrossRef] [PubMed]